Challenge Journal of STRUCTURAL MECHANICS

Vol.4 No.1 (2018)

buckling building codes columns continuous girder bridge durability dynamic analysis dynamic response earthquake finite element analysis finite element method meridional stresses operational modal analysis optimization reinforced concrete seismic analysis seismic design seismic isolation seismic response shallow foundations smart concrete teaching-learning based optimization

ISSN 2149-8024

TULPAR ACADEMIC PUBLISHING

Challenge Journal of Structural Mechanics

E-mail: *cjsmec@challengejournal.com*

Web page: *cjsmec.challengejournal.com*

TULPAR Academic Publishing
www.tulparpublishing.com

Challenge Journal of Structural Mechanics

CONTENTS

Research Articles

TULPAR ACADEMIC PUBLISHING

Challenge Journal of Structural Mechanics

Research Article

Influencing factors on effective width of compressed zone in joint column - cylindrical shell of steel silo

Lyubomir A. Zdravkov *

Department of Metal, Wood and Plastic Structures, University of Architecture, Civil Engineering and Geodesy (UACEG), Sofia 1046, Bulgaria

ABSTRACT

In order to ensure unloading of whole amount of stored product by gravity, steel silos are often placed on supporting structure. The simplest way to design these complicated facilities is to divide cylindrical shell on two parts in our minds - discretely supported ring beam and continuously supported shell above it. Obviously, to ensure continuously support of shell, bending stiffness of ring beam should be high. In European standard EN 1993-4-1, that concept is recognized but it keeps silence about recommended stiffness of ring beam. Another way to design is to know law of distribution of compressive axial stresses due to discrete column reactions R, by height of shell. Knowing it, we could calculate the effective width l_{eff} of distribution of compressive stresses on every level. Where effective width is equal to distance between discrete supports, there critical height of shell ends and above it cylindrical body is continuously supported. Unfortunately the above quoted standard EN 1993-4-1 does not give an information how to calculate l_{eff}. The questions here are; should we accept linear distribution of compressive forces by height? In addition, could we use directly the results of Whitmore (1952), where angle of distribution α = 30°? Or, even to accept a far more brave opinion that α = 45°, used by many of the elder designers? Moreover, is value of angle α constant or does it depend on various influencing factors?

ARTICLE INFO

Article history:
Received 11 May 2017
Revised 28 December 2017
Accepted 8 January 2018

Keywords:
Steel silo
Buckling
Meridional stresses
Angle of distribution
Effective width

1. Introduction

Steel silos are often placed on supporting structure. The purpose is easily and completely unload of all stored product by gravity. For every project the supporting structure is different, depending on real conditions of exploitation. Traditionally in Bulgaria were designed and executed supporting structures composed by 4 columns and horizontal girders between them, see Fig. 1a). Lately, under the influence of foreign designers, we can see other types of supporting structures, composed by columns only and vertical braces between them, see Fig. 1b).

Independently of type of supporting structure - built from girders and columns, or from columns only, it causes concentrated meridional forces in the cylindrical body of the silo. As a result, the thin shell could loses local stability.

The simplest way to design steel silos is to divide in our minds cylindrical shell on two parts - discretely supported ring beam and continuously supported shell above it. Obviously, to ensure continuously support of shell, bending stiffness of ring beam should be high. In European standard EN 1993-4-1 that concept is recognized but it keeps silence about recommended stiffness of ring beam. Rotter (1985) suggested that a value of ratio between stiffness of cylindrical shell and ring beam ψ=0.25 might be suitable for adoption in design.

Another approach to design steel silos is to know law of distribution of compressive axial stresses due to discrete column reactions R, by height of shell. Knowing the law, we could calculate effective width l_{eff} of distribution of compressive stresses on every level. Where effective width is equal to distance between discrete supports, there critical height of shell ends and above it cylindrical body is continuously supported. If the low is

* *Corresponding author*. Tel.: +359-885-081-305 ; E-mail address: zdravkov_fce@uacg.bg (L. A. Zdravkov)
ISSN: 2149-8024 / DOI: https://doi.org/10.20528/cjsmec.2018.01.001

simple, linear, we should know an angle α of distribution to the vertical axis only, see Fig. 2. Values of the angle α are of essential importance. Obviously as bigger would be the angle α as bigger would be the effective width l_{eff}, respectively meridional stress $\sigma_{x,Ed}$ will be smaller.

a) columns and horizontal girders between them

b) columns with circular sections only vertical braces between them

Fig. 1. Variations of supporting structure under the silo.

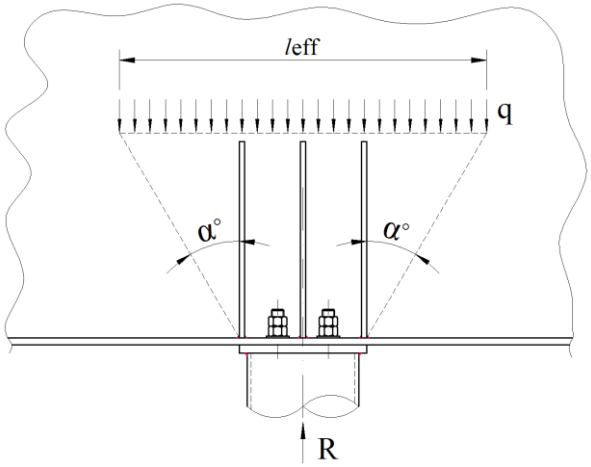

Fig. 2. Angle α of the distribution of compressive forces in the cylindrical shell and effective width l_{eff} if law is linear.

Unfortunately corresponding standards EN 1993-1-6:2007 and EN 1993-4-1:2007 do not give information about the values of the angle α and respectively of l_{eff}. Maybe because they are focused on idea about ring beam. Only in the standard EN 1993-1-5:2006 we can find a formula for determining l_{eff} due to concentrated force in the plain of the steel plate. The equation is as following:

$$l_{\text{eff}} = s_e\sqrt{1+\left(\frac{z}{n\cdot s_e}\right)^2}\,, \tag{1}$$

in which:

$$s_e = s_s + 2t_f, \tag{2}$$

$$n = 0.636\sqrt{1+\frac{0.878\cdot a_{st,1}}{t_w}}, \tag{3}$$

where s_s is the width of a loading patch; t_f – thickness of flange where the force is applied; t_w - thickness web of the steel plate; z – distance from the flange to the studied section; $a_{st,1}$ – surface of the gross cross section of the stiffeners, put on the length s_e.

Eq. (1) is valid when the inequality (4) is valid. In another case the contribution of the stiffeners should be ignored.

$$\frac{s_{st}}{s_e} \le 0.5\,, \tag{4}$$

where s_{st} is the axial distance between the stiffeners.

The question here is whether the formula (1) for plain plates is valid also for cylindrical shells such as the silos? Or to accept simple linear distribution, see Fig. 2 and use directly the results of Whitmore (1952), published in distant 1952, showing angle α=30^0? Or even to accept far more brave opinion that α=45^0 used by many of the elder designers?

2. Research of Joint Cylinder - Supporting Structure

In order to find the answer of all these questions above, the author developed several spatial research models of different silos. Software SAP 2000 v.14.2 is used in the research. All elements in numerical models of the facilities were introduced as shells with their real thickness. In order to reduce time for computer calculations, the supporting structure was replaced by unmovable hinge supports. They are 8 pcs. per silo, equally spaced by circumference of shell. Width of each support varies by silo.

Discharging conical hopper of silos is joined to the cylindrical shell at some distance above his lower end, see Fig. 3. This solution is classical. It permits to the girders or columns of the supporting structure to be placed exactly under the cylindrical shell, i.e. there will not be generated additional torsional or bending moments.

In order to study the effect of every one of influencing factors, research is conducted by different constructive solutions for the joints, as follow:

a) The silo is composed by cylindrical shell only, without a discharging conical hopper and without vertical stiffeners above supports, see Fig. 4a). In two separate cases, on vertical shell are applied loads as follow:

- Vertical load P_{we}(z) only, due to friction of a stored product to the shell;
- Initially the shell is loaded by radial pressure P_{he}(z), caused by product. After that, in deformed by P_{he}(z) condition, is applied load P_{we}(z) due to the friction.

b) Conical discharging hopper is added to cylindrical shell. There are not vertical stiffening elements, see Fig. 4b). In two separate cases, on vertical shell are applied the same loads, described above, in point a);
c) The silo is composed by cylindrical shell without discharging hopper. Vertical stiffeners are placed on shell, above supports, see Fig. 4c). In two separate cases, on vertical shell are applied the same loads, described above, in point a);
d) The silo is composed by cylindrical shell and a discharging hopper. Vertical stiffeners are placed above supports, see Fig. 4d). In two separate cases, on vertical shell are applied the same loads, described above, in point a);
e) The silo is composed by cylindrical shell and a discharging conical hopper. Vertical stiffeners are placed above supports, see Fig. 4d). In two separate cases, on vertical shell and conical hopper are applied loads as follow:
- Vertical load $P_{we}(z)$ on the shell and meridional load $P_{te}(z)$ on the hopper. The loads are caused by friction of the product to the steel structure;
- Initially the shell is loaded by radial pressure $P_{he}(z)$ and respectively conical hopper - by normal pressure $P_{ne}(z)$. After that, in the deformed by loads $P_{he}(z)$ и $P_{ne}(z)$ condition, the friction loads $P_{we}(z)$ and $P_{te}(z)$ are applied.

Loads $P_{we}(z)$, $P_{te}(z)$, internal pressure $P_{he}(z)$, $P_{ne}(z)$, friction loads $P_{we}(z)$ and $P_{te}(z)$, are calculated for real stored products, according to standard EN 1991-4.

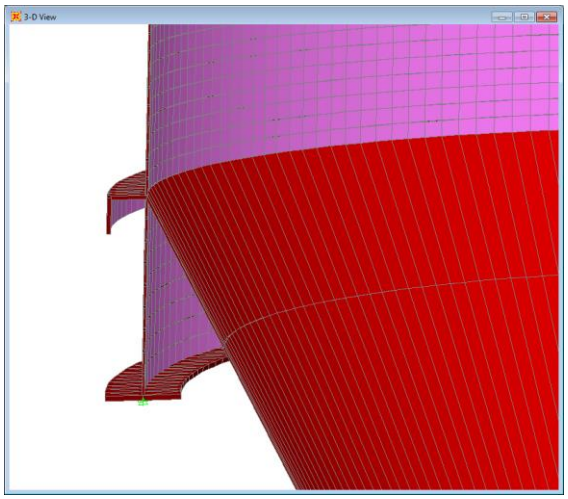

Fig. 3. Joint of cylindrical shell with a cone hopper.

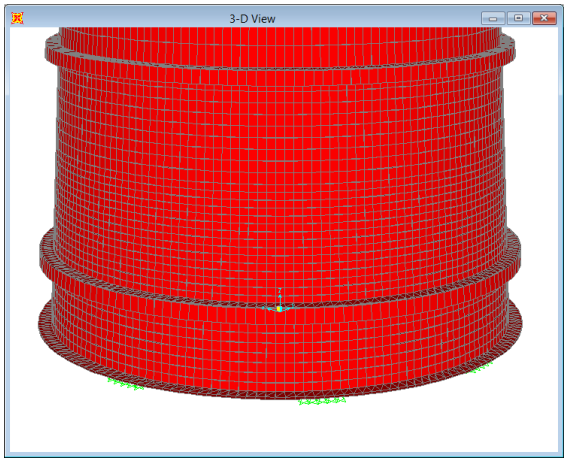

a) cylindrical shell only

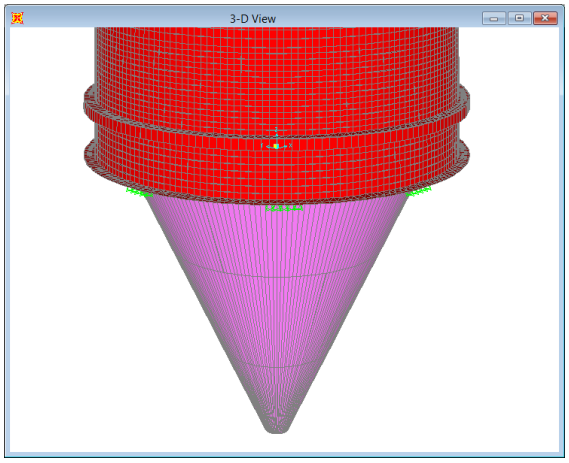

b) cylindrical shell and a conical hopper, without vertical stiffening plates

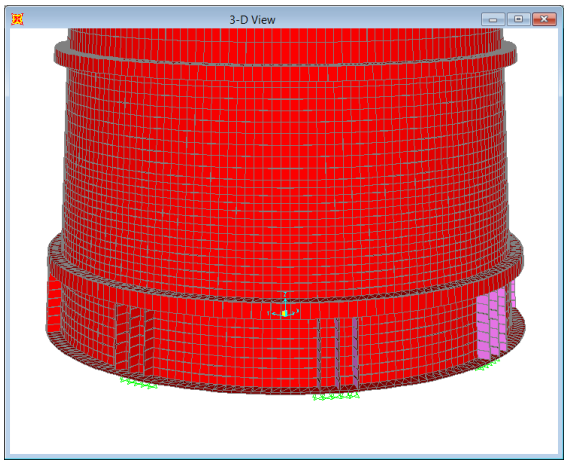

c) cylindrical shell and vertical stiffeners

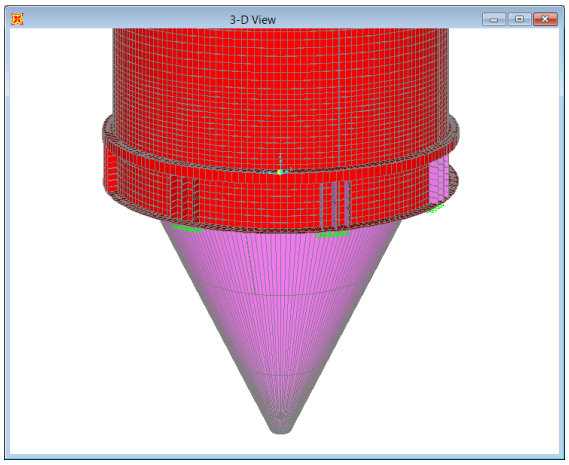

d) cylindrical shell and a conical hopper vertical stiffening plates were placed on shell

Fig. 4. Variants of researched silos and joints.

Normal meridional stresses $\sigma_{x,Ed}$ caused by vertical load $P_{we}(z)$, are measured in points in first course, above stiffening ring. As we know value of the shell's thickness t and value of the reaction R in support, effective width l_{eff} can be calculated according to formula:

$$l_{\text{eff}} = \frac{R-\Delta F}{\sigma_{x,Ed} \cdot t}, \quad (5)$$

where R is a vertical reaction in the discrete support, see Fig. 2, caused by the vertical load $P_{we}(z)$, due to friction of a stored product to the shell; $\sigma_{x,Ed}$ – normal meridional stress in the cylindrical shell, above joint between cylinder and conical hopper; t – thickness of the cylindrical steel shell in the joint cylinder - conical hopper; ΔF – force, caused by the friction on the shell with a height Δh. It could be calculated by the formula:

$$\Delta F = \frac{2\pi r_i \cdot \Delta h \cdot P_{we}(z)}{n_s}, \quad (6)$$

where r_i is the radius of the internal surface of the cylindrical shell; Δh – the distance between the point of measurement of normal stresses $\sigma_{x,Ed}$ and the joint between cylinder and conical hopper; n_s – number of supports in the cylindrical shell.

The angle α of distribution of normal stresses in shell, due to reactions R in supports, could be calculated according to formula:

$$\alpha = \text{arctg}\left(0.5\frac{l_{eff}-b_s}{h}\right), \quad (7)$$

in which b_s is the width of the support; h – vertical distance between point of applying of reactions R and point of measurement of meridional normal stresses $\sigma_{x,Ed}$.

In all models is used steel S235, with a properties according to standard EN 10025-2:2004.

Buckling Analysis option is activated in used software SAP 2000 v.14.2. This option allows to determine reserve of bearing capacity k of the cylindrical shell before buckling, partly or entirely. Multiplication the result of total vertical reactions and the reserve of the bearing capacity k gives the value of the total meridional critical force ΣR_{cr} in which perfect shell will loses stability in the elastic condition. In this case meridional elastic critical buckling stress $\sigma_{x,Rcr}$ could be calculated according to the formula:

$$\sigma_{x,Rcr} = \frac{\Sigma R_{cr}}{2\pi r t}, \quad (8)$$

where r is the radius of the middle surface of cylindrical shell.

Critical normal stresses $\sigma_{x,Rcr}$ and calculated through them design meridional critical stresses $\sigma_{x,Rd}$ give quantitative assessment of the influence of different solutions of base joints on the stability of the shell.

3. Results of the Research of Joint of Cylindrical Shell - Supporting Structure

3.1. Silo № 1

volume V = 110 m³
stored product - slack lime;
diameter D = 3 492 mm;
height h_c = 10 950 mm;
thickness of 1st course $t_{s,1}$ = 6 mm;
width of supports - b_s = 240 mm.

Case		Buckling factor k	Element which loses stability	l_{eff} cm	α deg.
1	a)	12,7561	1st course, above the column, under the stiffening ring	104,1	33,8
	b)	12,7520		104,1	33,8
2	a)	12,7813		105,3	34,2
	b)	12,7776		105,2	34,2
3	a)	24,46960	1st course, above vertical stiffeners and stiffening ring	75,1	23,1
	b)	24,59327		75,1	23,1
4	a)	25,14499		82,5	26,1
	b)	25,28706		82,5	26,1
5	a)	23,75416		82,5	26,1
	b)	23,79654		82,5	26,1

3.2. Silo № 2

volume V = 110 m³
stored product - slack lime;
diameter D = 3 492 mm;
height h_c = 10 950 mm;
thickness of 1st course $t_{s,1}$ = 4 mm;
width of supports - b_s = 240 mm.

Case		Buckling factor k	Element which loses stability	l_{eff} cm	α deg.
1	a)	5,44410	1st course, above the column, under the stiffening ring	107,1	34,8
	b)	5,44095		107,1	34,8
2	a)	5,44872		108,4	35,2
	b)	5,44601		108,4	35,2
3	a)	10,34025	1st course, above vertical stiffeners and stiffening ring	80,8	25,4
	b)	10,43100		80,8	25,4
4	a)	10,72707		81,8	25,8
	b)	10,83076		81,8	25,8
5	a)	10,07763		81,9	25,8
	b)	10,08339		81,8	25,8

3.3. Silo № 3

volume V = 40 m³
stored product - grained (fine) fraction of sand;
diameter D = 2 500 mm;
height h_c = 8 470 mm;
thickness of 1st course $t_{s,1}$ = 6 mm;
width of supports - b_s = 230 mm.

Case		Buckling factor k	Element which loses stability	l_{eff} cm	α deg.
1	a)	21,45635	1st course, above the column, under the stiffening ring	79,8	33,4
	b)	21,44135		79,8	33,4
2	a)	21,41201		81,9	34,3
	b)	21,40105		81,9	34,3
3	a)	23,84189	2nd course, above vertical stiffeners and stiffening ring. 1st course does not buckle	67,8	27,8
	b)	24,04884		67,8	27,8
4	a)	23,96794		73,0	30,3
	b)	24,14155		73,0	30,3
5	a)	23,75764		72,98	30,3
	b)	23,97564		72,98	30,3

3.4. Silo № 4

volume V = 40 m³
stored product - grained (fine) fraction of sand;
diameter D = 2 500 mm;
height h_c = 8 470 mm;
thickness of 1st course $t_{s,1}$ = 4 mm;
width of supports - b_s = 230 mm.

Case		Buckling factor k	Element which loses stability	l_{eff} cm	α deg.
1	a)	9,41556	1st course, above the column, under the stiffening ring	81,4	34,0
	b)	9,40196		81,4	34,0
2	a)	9,38163		83,4	34,9
	b)	9,37208		83,4	34,9
3	a)	18,47540	1st course, above vertical stiffeners and stiffening ring	66,4	27,1
	b)	18,45486		66,4	27,1
4	a)	19,04036		71,9	29,8
	b)	19,01426		71,9	29,8
5	a)	18,24653		71,9	29,8
	b)	18,15925		71,9	29,8

3.5. Silo № 5

volume V = 150 m³
stored product - sand;
diameter D = 4 500 mm;
height h_c = 8 940 mm;
thickness of 1st course $t_{s,1}$ = 8 mm;
width of supports - b_s = 350 mm.

Case		Buckling factor k	Element which loses stability	l_{eff} cm	α deg.
1	a)	12,35903	1st course, above the column, under the stiffening ring	162,5	37,2
	b)	12,16633		162,5	37,2
2	a)	12,37384		163,3	37,4
	b)	12,17882		163,3	37,4
3	a)	20,57089	2nd course, above vertical stiffeners and stiffening ring. 1st course does not buckle	131,3	29,8
	b)	20,76019		131,3	29,8
4	a)	20,64411		140,1	32,1
	b)	20,80852		140,1	32,1
5	a)	19,98260		140,08	32,0
	b)	20,19925		140,07	32,0

3.6. Silo № 6

volume V = 150 m³
stored product - sand;
diameter D = 4 500 mm;
height h_c = 8 940 mm;
thickness of 1st course $t_{s,1}$ = 5 mm;
width of supports - b_s = 350 mm.

Case		Buckling factor k	Element which loses stability	l_{eff} cm	α deg.
1	a)	4,76692	1st course, above the column, under the stiffening ring	166,5	38,1
	b)	4,62667		166,5	38,1
2	a)	4,77424		166,1	38,0
	b)	4,63235		166,1	38,0
3	a)	11,13561	1st course, above vertical stiffeners and stiffening ring	125,2	28,2
	b)	10,96758		125,3	28,3
4	a)	11,31482		135,9	31,0
	b)	11,14099		135,9	31,0
5	a)	10,06433	1st course, between vertical stiffeners	135,9	31,0
	b)	9,94094		135,9	31,0

Graphics in Fig. 5 show how the angle of distribution α changes on the height of cylindrical shell. Points (joints) where the measurements were done, are situated in the 1st course, above the joint between cylinder – conical hopper.

Obviously the value of angle α is not constant, it decrease by height. In other words, distribution of compressive forces by height is not linear. Zdravkov (2017a; 2017b) made similar conclusion in another research. Fortunately the effective width l_{eff} increases, see Fig. 6. Practical consequence is that if the values for l_{eff} are determined for a point close above the joint between cylinder – conical hopper, these values will be conservative, on side of safety for next manual (algebraic) calculations.

The above mentioned results show that, when vertical distance above base increases, the influence of various stiffening elements decrease. Values of α and l_{eff} going to be practically the same on higher level.

Influence of the conical discharging hopper is positive in all researched silos, but its contribution is a small. The most probably it is due to:
- all studied models have stiffening ring on point where cylindrical shell and the hopper joint;
- all researched models have relatively close spaced 8 supports.

More significant is effect of using of vertical stiffening elements. They considerably increase the bearing capacity of cylindrical shell subjected to meridional pressure by patch loads. On other hand, angle of distribution α, respectively the effective width l_{eff}, are bigger when the shells do not have stiffeners, compared with stiffened shells. For preliminary manual calculations, averaged angle α could be accepted as follow:
- cylindrical shell, without vertical stiffeners above the discrete supports - α = 34° ÷ 36°;
- cylindrical shell with vertical stiffeners above the discrete supports - α = 26° ÷ 30°.

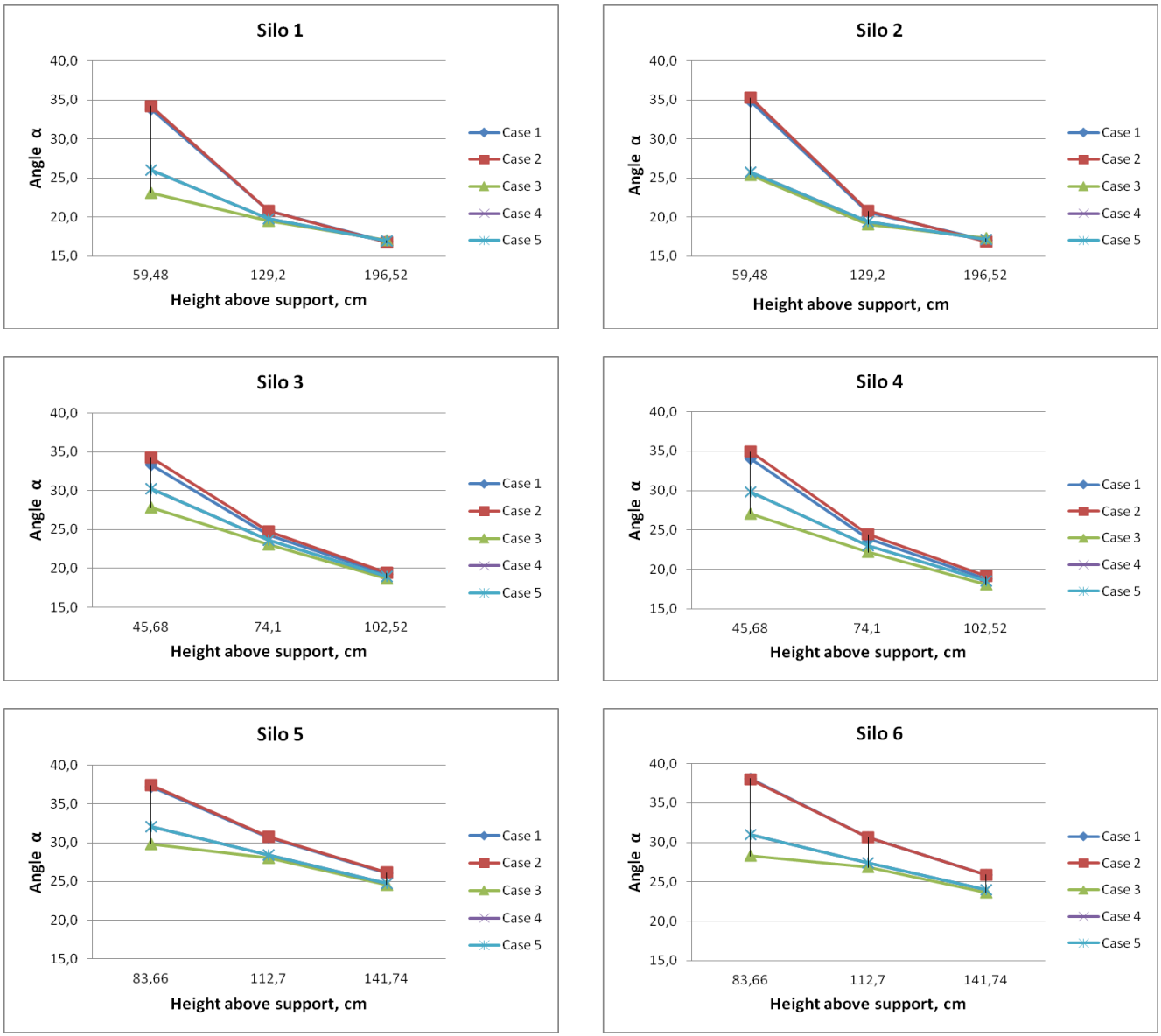

Fig. 5. Change of angle of distribution α of normal stresses $\sigma_{x,Ed}$ on the height of the cylindrical shell.

In studied there 6 models of silos, everyone with 5 variants, are not reported an averaged angle $\alpha \approx 45°$. Maybe because all skirts of silos, respectively points of measurements, are relative height. Knoedel and Ummenhofer (2009) claim that value $\alpha \approx 45°$ can be obtained when the stiffening ring is enough rigid.

As we can notice, the distribution angle α decreases when the ratio of D/t_s increases. Similar correlation is noticed by Knoedel and Ummenhofer (1998) in another research.

Internal pressures $P_{he}(z)$ and $P_{ne}(z)$ do not have noticeable influence on angle α and l_{eff} if the joint cylinder – conical hopper is made as is shown on the Fig. 3.

The courses of the researched here silos have various thickness. They decrease from lower to the higher parts, which is related with the different values of internal pressure on them. In some of the silos, like Silo №3 and Silo №4, buckles not the lowest 1st course, under which are the supports, but the upper 2nd course, which is thinner, see Fig. 7. It means that in silos with stepped wall thickness is not sufficient to study only loaded by the concentrated meridional forces the lowest 1st course. The thinner upper courses also should be checked. And here again appears the problem for the value of the effective width l_{eff} in horizontal joint of the 1st and 2nd course and how to determine it correctly.

4. Conclusions

Design of steel silos is a complicated and responsible task. The difficulties become more serious when the silos are elevated and supports beneath are discrete. One of most discussed question is how to calculate effective width l_{eff} of compressive meridional stresses above supports. Unfortunately the responsive standards EN 1993-1-6:2007 and EN 1993-4-1:2007 do not give an answer of this question. Obviously influencing factors are a lot of and could not be included in one formula. Therefore it is not correct shown in EN 1993-1-5: 2006 formulae to be applied in silos.

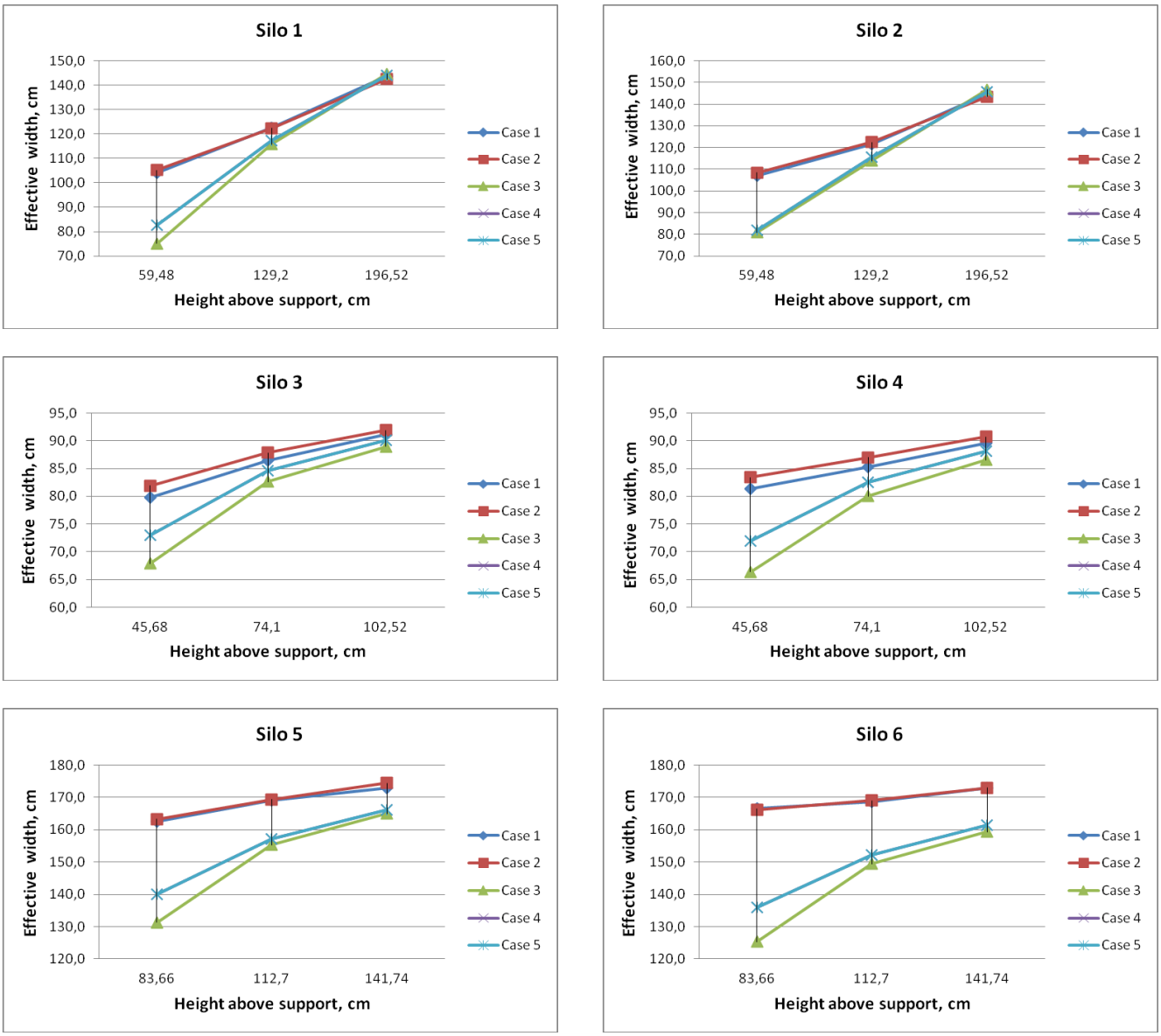

Fig. 6. Change of effective width l_{eff} of compressive stresses $\sigma_{x,\text{Ed}}$ by height of the cylindrical shell.

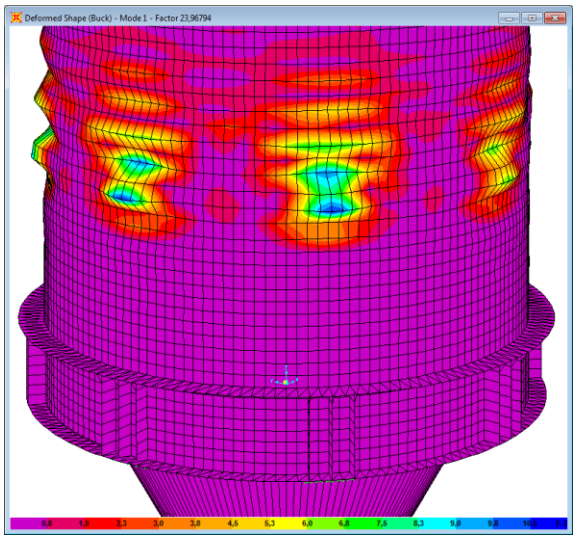

Fig. 7. The loss of stability in the cylindrical shell of the silos in thinner 2nd course.

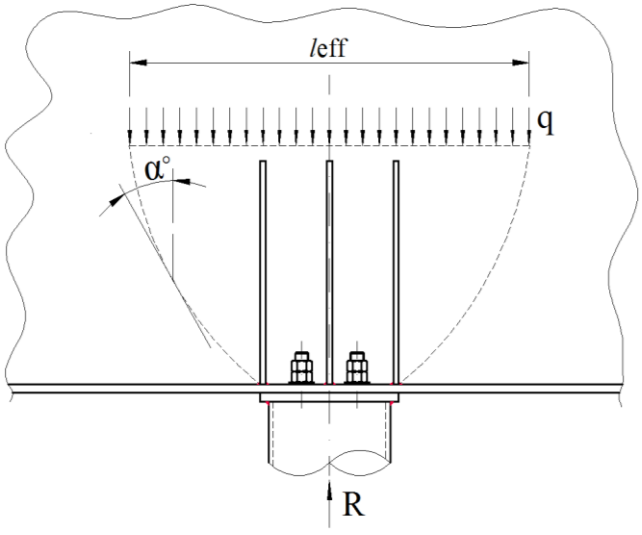

Fig. 8. Real distribution of compressive forces in the cylindrical shell and effective width l_{eff}.

The main outcomes from the current research of 6 silos on 8 supports are:

- The value of angle α is not constant, it decreases by height. Real distribution of compressive forces looks like as is shown on Fig. 8.
- The vertical stiffeners above the supports have considerable influence of angle of distribution α and effective width l_{eff}. For preliminary manual calculations, the averaged angle α could be accepted as follow:
- cylindrical shell, without vertical stiffeners above the supports - $\alpha = 34° \div 36°$;
- cylindrical shell with vertical stiffeners above the supports - $\alpha = 26° \div 30°$.
- The angle of distribution α decreases when the ratio D/t_s increases.
- When there is a stiffening ring in joint cylindrical shell – hopper, the influence of hopper is very small.
- In joint cylinder - conical hopper as is shown on the Fig. 3, internal pressure does not have a noticeable effect on angle α and l_{eff}.

REFERENCES

EN 1991-4:2006 (2006). Eurocode 1 - Actions on structures - Part 4: Silos and tanks, European committee for standardization, Brussels.

EN 1993-1-5:2006 (2006). Eurocode 3 - Design of steel structures - Part 1-5: Plated structural elements. European Committee for Standardization, Brussels.

EN 1993-1-6:2007 (2007). Eurocode 3 - Design of steel structures - Part 1-6: Strength and Stability of Shell Structures. European Committee for Standardization, Brussels.

EN 1993-4-1:2007 (2007). Eurocode 3 - Design of steel structures - Part 4-1: Silos. European Committee for Standardization, Brussels.

EN 10025-2:2004 (2004). Hot rolled products of structural steels - Part 2: Technical delivery conditions for non-alloy structural steels. European Committee for Standardization, Brussels.

Knödel P, Ummenhofer T (1998). Ein einfaches Modell zum Stabilitätsnachweis zylindrischer Schalentragwerke auf Einzelstützen. *Stahlbau*, 67, 425-429.

Knödel P, Ummenhofer T (2009). Silos with stepped wall thickness on local supports. *Proceedings of the International Association for Shell and Spatial Structures (IASS) Symposium*, Valencia.

Rotter JM (1985). Analysis and Design of Ringbeams. *Design of steel bins for storage of bulk solids*, J. M. Rotter, ed., University of Sydney, Sydney, Australia, 164-183.

SAP 2000 v.14.2. Structural analysis program. Computers and Structures, Inc.

Whitmore RE (1952). Experimental Investigation of Stresses in Gusset Plates. Bulletin No. 16, Engineering Experiment Station, University of Tennessee, Knoxville, USA.

Zdravkov LA (2017a). Some specific features of design of steel silo with capacity V = 110 m^3. *International Jubilee Scientific Conference "75th Anniversary of UACEG"*, Sofia.

Zdravkov LA (2017b). Influence of intermediate rings and height of skirt on effective width of compression zone in junction column - cylindrical shell of steel silo. *International Jubilee Scientific Conference "75th Anniversary of UACEG"*, Sofia.

Challenge Journal of Structural Mechanics

Research Article

Mechanical performance comparison of glass and mono fibers added gypsum composites

Sadık Alper Yıldızel *, Serdar Çarbaş

Department of Civil Engineering, Karamanoğlu MehmetBey University, 70100 Karaman, Turkey

ABSTRACT

Gypsum and gypsum based composite are widely preferred in construction industry for various purposes. Mechanical performances of gypsum composite have been enhanced by researchers in order to increase its area of usage. In this research, gypsum composites containing expanded glass were reinforced by glass fibers (GF) and mono polypropylene fibers (MPF). GF and MPF were used up to 1.5%. The flexural strength, compressive strength, and shrinkage behavior of the composites were examined within the scope of this study. 50 x 50 x 50 mm and 40 x 40 x 160 sized specimens were prepared for the mechanical performance tests. It was obtained that flexural and shrinkage behavior of the composite were enhanced with the addition of MPF compared to GF added mixes; however, compressive strength values were not as high as GF reinforced composites.

ARTICLE INFO

Article history:
Received 8 November 2017
Revised 7 December 2017
Accepted 18 December 2017

Keywords:
Gypsum
Gypsum composite
Glass fiber
Mono propylene fiber
Mechanical properties

1. Introduction

Gypsum composites are widely used in the construction industry depending on their good sound insulation, thermal and fire resistance properties (Gazineu et al., 2011; Heim et al., 2004; Li et al., 2011; Vimmrova et al., 2011). Different types of materials can be added for enhancing mechanical properties of the gypsum based composites (Eve et al., 2002). Among various types and sizes, fibers are effectively used for the improvement of the mechanical properties (Yu et al., 2012; Wu, 2004; Colak, 2006).

Reinforcement fibers can be classified into two groups: natural fibers and manufactured fibers. Flax and wool can be counted as natural fibers. And basalt, carbon, glass fibers are in the group of man-made fibers. Man-made fibers were used in this research. Glass fibers are widely preferred by the academics for producing gypsum composites (Medina and Barbero-Barrera, 2017). While producing GF reinforced composite panels, the use of GF cannot be counted as conventional. Traditional design criteria are not always applicable due to the usage of this type of fiber. Many researches have been conducted for better understanding of its structural behavior (Liu et al., 2008; Janardhana et al.,2007; Wu and Dare, 2006). Especially, shrinkage behavior of the gypsum composites is one of the main research topics (Zhao et al., 2008).

MPF were also added to the gypsum composites for improving mechanical properties (Tazawa, 1998). MPF are widely used for their high specific performances and low costs. They can also be added into the matrix as forming layers or frames (Eve, 2002; Medina and Barbero-Barrera, 2017). Numerous researches have been conducted to emphasize the importance of adding MPF into the gypsum based composites in the construction industry (Deng and Furuno, 2001; Martias, 2014).

2. Material and Experimental Method

Gypsum mixes were prepared as per the requirements of the Turkish standard TS EN 13279-1. The characteristic properties of the gypsum can be seen in Table 1. Expanded glass was used as aggregate. Properties of the expanded glass can be found in Table 2. Alkali resistant GF and MPF with the length of 10 mm were used for the experimental studies. The fiber properties are presented in Table 3.

* *Corresponding author*. Tel.: +90-338-2262000 ; Fax: +90-338-2262214 ; E-mail address: sayildizel@kmu.edu.tr (S. A. Yıldızel)
ISSN: 2149-8024 / DOI: https://doi.org/10.20528/cjsmec.2018.01.002

Table 1. Characteristic properties of the gypsum

Characteristic properties	
Compressive strength (MPa)	2.7
Flexural strength (MPa)	1.3
Dry density (kg/m^3)	800 – 1000
Workability time (min)	70 -95
Final setting time (min)	130

Table 2. Expanded glass properties

Expanded glass	
Specific weight (g/cm^3)	0.19 – 0.4
Compressive strength (MPa)	1.4 – 2.6
Water absorption by volume	7-19
pH	9-12
Color	white

Table 3. GF and MPF properties

GF		MPF	
Ultimate strength, bending (MOR, MPa)	20-28	Specific gravity	0.91
Elastic limit (LOP, MPa)	7-11	Tensile strength (MPa)	590
Compressive strength (MPa)	50-80	N/A	N/A
Modulus of elasticity (GPa)	10-20	N/A	N/A
Density (kg / m^3)	1870 - 2100	Density (kg / m^3)	910
Alkali resistant	excellent	Alkali resistant	excellent

Mix proportions and the experimental sets were given in Table 4. The gypsum was replaced with the expanded glass by 7.5% by weight of gypsum. The materials were mixed in a mixer for 3 minutes to for a better homogenous dry mixture. GF and MPF were added with water after this process and mixed for 5 minutes. The fibers were used at the ratios of 1%, 1.25% and 1.5% in the mix design. Polycarboxylate based plasticizer was selected as the chemical agent. Water/ binder ratio was kept constant at the value of 0.45 in order to obtain the stable mix..

Table 4. Mixture designs

Mixture Code	Gypsum (kg)	Expanded glass (kg)	GF (%)	MPF (%)	Water / binder ratio
GF-1	46.25	3.75	1	-	0.45
GF-2	46.25	3.75	1.25	-	0.45
GF-3	46.25	3.75	1.5	-	0.45
MPF-1	46.25	3.75	-	1	0.45
MPF-2	46.25	3.75	-	1.25	0.45
MPF-3	46.25	3.75	-	1.5	0.45

All prepared specimens were kept at the molds for 24 hours at the room temperature, and potable water was used for the mixes. Compressive and flexural strength of the samples were measured for 1, 7 and 28 days according to the TS EN 13279-2 standards. Shrinkage test was conducted with the help of laser based shrinkage test tool. The dimensional changes were recorded for 24 hours.

3. Results and Discussions

Mechanical properties of the composites were presented in this section. The compressive and flexural test results of the specimens are given in Figs. 1 and 2, respectively.

Compressive strength results showed that compressive strength values increase with the increase of each fiber ratios. However, GF reinforced gypsum composites results are higher compared to the MPF reinforced specimens. As seen in Fig 1, test results were complied with the similar literature researches (Medina and Barbero-Barrera, 2017; Martias, 2014). However, the results of other relevant studies are also confusing for the compressive strength values, this situation can be the effect of the size and the direction of the fibers.

As expected, the flexural strength values are increased with the increasing fiber ratio. Moreover, MPF added gypsum composites showed a better performance compared to GF reinforced mixes.

The shrinkage behavior of the gypsum composites can be found in Fig. 3. It was observed that dimensional stability of the MPF added composites are better against the GF added ones.

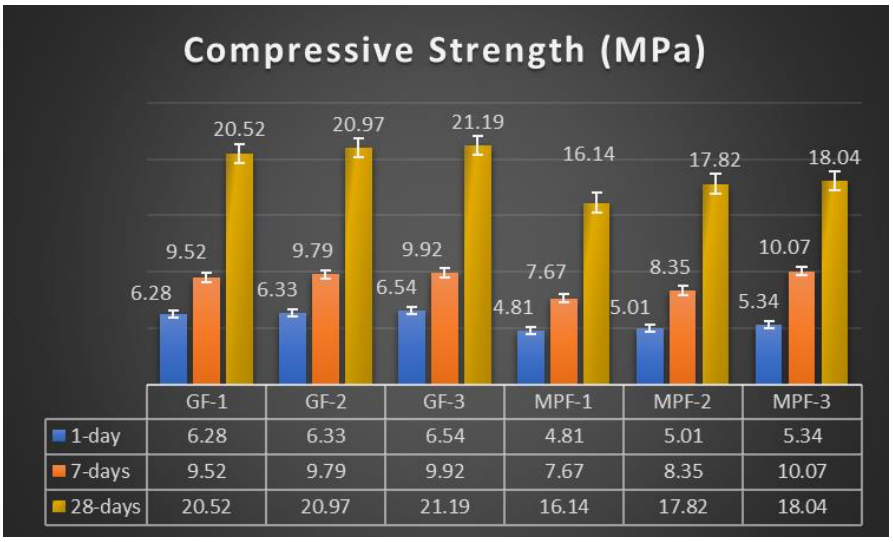

Fig. 1. Compressive strength test results.

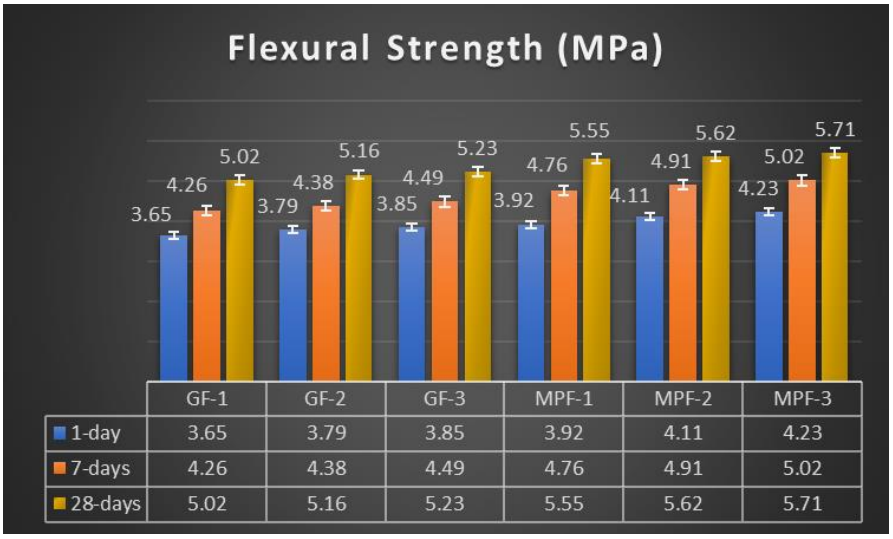

Fig. 2. Flexural test results.

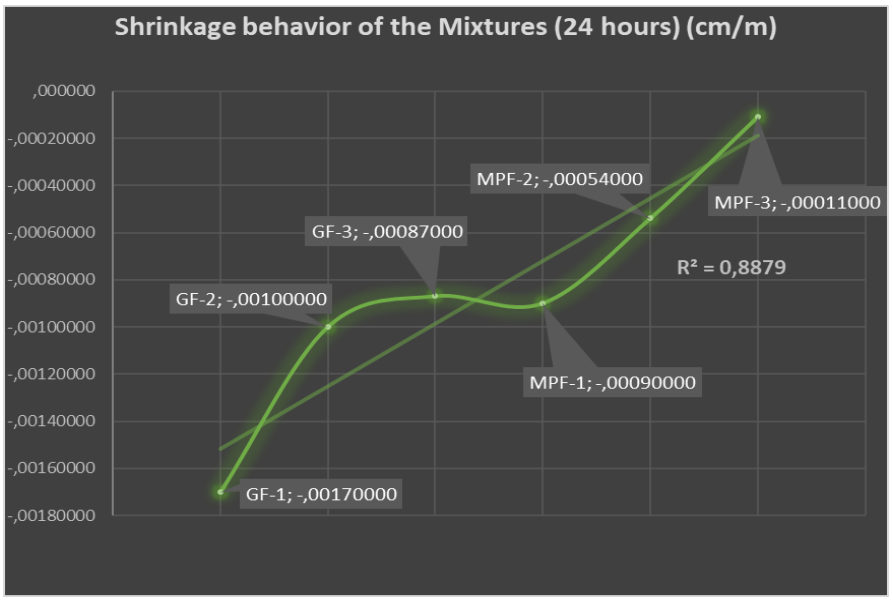

Fig. 3. Shrinkage behavior.

4. Conclusions

Gypsum based composites with GF and MPF have been analyzed for the mechanical performances and the comparison. The main findings can be summarized as follows:

- The increase in fiber ration in gypsum composites increases the mechanical strength values of the mixes.
- The MPF added gypsum composites showed better performances when analyzing flexural and shrinkage behavior of the designs; however, GF reinforced composites compressive strength values are higher.
- A good synergy was obtained between the MPF and gypsum based composites in respect to limiting shrinkage movements.
- Addition of 1.5% MPF presents the mechanical results for the gypsum composites.
- MPF can be preferred in replacement of GF due to their low cost and high specific performances in gypsum composite applications.

REFERENCES

Çolak A (2006). Physical and mechanical properties of polymer-plaster composites. *Materials Letters*, 60(16), 1977-1982.

Eve S, Gomina M, Gmouh A, Samdi A, Moussa R, Orange G (2002). Microstructural and mechanical behaviour of polyamide fibre-reinforced plaster composites. *Journal of the European Ceramic Society*, 22(13), 2269-2275.

Gazineu MHP, Dos Santos VA, Hazin CA, De Vasconcelos WE, Dantas CC (2011). Production of polymer-plaster composite by gamma irradiation. *Progress in Nuclear Energy*, 53(8), 1140-1144.

Heim D, Clarke JA (2004). Numerical modelling and thermal simulation of PCM–gypsum composites with ESP-r. *Energy and Buildings*, 36(8), 795-805.

Li M, Wu Z, Chen M (2011). Preparation and properties of gypsum-based heat storage and preservation material. *Energy and Buildings*, 43(9), 2314-2319.

Martias C, Joliff Y, Favotto C (2014). Effects of the addition of glass fibers, mica and vermiculite on the mechanical properties of a gypsum-based composite at room temperature and during a fire test. *Composites Part B: Engineering*, 62, 37-53.

Medina NF, Barbero-Barrera MM (2017). Mechanical and physical enhancement of gypsum composites through a synergic work of polypropylene fiber and recycled isostatic graphite filler. *Construction and Building Materials*, 131, 165-177.

Tazawa EI (1998). Effect of self-stress on flexural strength of gypsum-polymer composites. *Advanced Cement Based Materials*, 7(1), 1-7.

TS EN 13279-1 (2014). Gypsum binders and gypsum plasters–Part, 1. Turkish Standards Institute, Ankara.

TS EN 13279-2 (2015). Gypsum Binders and Gypsum Plasters–Part, 2. Turkish Standards Institute, Ankara.

Vimmrova A, Keppert M, Svoboda L, Černý R (2011). Lightweight gypsum composites: Design strategies for multi-functionality. *Cement and Concrete Composites*, 33(1), 84-89.

Wu YF (2004). The effect of longitudinal reinforcement on the cyclic shear behavior of glass fiber reinforced gypsum wall panels: tests. *Engineering Structures*, 26(11), 1633-1646.

Wu YF, Dare MP (2006). Flexural and shear strength of composite lintels in glass-fiber-reinforced gypsum wall constructions. *Journal of Materials in Civil Engineering*, 18(3), 415-423.

Yu QL, Brouwers HJH (2012). Development of a self-compacting gypsum-based lightweight composite. *Cement and Concrete Composites*, 34(9), 1033-1043.

Zhao K, Zhang X, Wei TJ (2008). Full-scale model test on the performance of a five-storey fiber plaster board building. *In: Proceedings of the seventh international RILEM symposium fiber reinforced concrete: design and applications (BEFIB-2008 symposium)*, Chennai, India, 17–19.

Challenge Journal of Structural Mechanics

Research Article

Seismic assessment of a curved multi-span simply supported truss steel railway bridge

Mehmet Fatih Yılmaz [a,*], Barlas Özden Çaglayan [b], Kadir Özakgül [b]

[a] *Department of Civil Engineering, Ondokuz Mayıs University, 55105 Samsun, Turkey*
[b] *Department of Civil Engineering, İstanbul Technical University, 34457 İstanbul, Turkey*

ABSTRACT

Fragility curve is an effective method to determine the seismic performance of a structural and nonstructural member. Fragility curves are derived for Highway Bridges for many studies. In Turkish railway lines, there are lots of historic bridges, and it is obvious that in order to sustain the safety of the railway lines, earthquake performance of these bridges needs to be determined. In this study, a multi-span steel truss railway bridge with a span length of 25.7m is considered. Main steel truss girders are supported on the abutments and 6 masonry piers. Also, the bridge has a 300m curve radius. Sap 2000 finite element software is used to model the 3D nonlinear modeling of the bridge. Finite element model is updating according to field test recordings. 60 real earthquake data selected from three different soil conditions are considered to determine the seismic performance of the bridge. Nonlinear time history analysis is conducted, and maximum displacements are recorded. Probabilistic seismic demand model (PSDMs) is used to determine the relationship between the Engineering Demand Parameter (EDP) and Intensity Measure (IMs). Fragility curve of the bridge is derived by considering the serviceability limit state, and results are discussed in detail.

ARTICLE INFO

Article history:
Received 18 November 2017
Revised 30 January 2018
Accepted 14 February 2018

Keywords:
Railway bridge
Earthquake performance
Fragility curve
Nonlinear analysis

1. Introduction

Turkey is under the influence of North Anatolia, Southeast Anatolia, and Western Anatolia earthquake zones. Therefore, 42% of the country is located in the very high seismic hazard zone. The railway lines in Turkey were started to build up in the 19th century. %82 of the bridges, and culverts were built before 1960 (Çağlıyan and Yıldız, 2013). To determine the seismic vulnerabilities of the bridges fragility curves must be derived. Fragility curve is a most used effective tool to determine the seismic performance of bridges. Fragility is the probability of a structural or nonstructural member which will exceed certain performance limit under an earthquake condition (Pan et al., 2010b). Fragility curves can be derived in three different way; Expert base, empirical and analytical (Shinozuka et al., 2000a; Nielson, 2005).

To derive expert base and empirical fragility curve past earthquake reports and expert opinion about the damage state of the bridge are a need. It is not possible to obtain this information for all bridges, so that the analytical method needed to derive the fragility curve becomes important. Linear and nonlinear analyses are being used to determine the relation between EDP and IM to derive analytical fragility curve. Nonlinear time history analysis is a frequently used and an effective tool to derive analytical fragility curve (Banerjee and Shinozuka, 2007; Bignell et al., 2004; Shinozuka et al., 2000b; Mackie and Stojadinovic, 2001; Kumar and Gardoni, 2014). Analytical fragility curves are also commonly used to determine the seismic performance of the bridges (Mackie and Stojadinovic, 2003; Pan et al., 2010a and 2010b; Shinozuka et al., 2007a and 2007b).

* *Corresponding author*. Tel.: +90-362-3121919 ; E-mail address: yilmazmehmet3@itu.edu.tr (M. F. Yılmaz)
ISSN: 2149-8024 / DOI: https://doi.org/10.20528/cjsmec.2018.01.003

In this study Bekdemir railway bridge is investigated. 60 different real earthquake data are selected, and non-linear time history analysis is performed to determine PSDMs. Fragility curve of the bridge is derived by using two-parameter log-normal distribution function. Serviceability limit states for three different serviceability velocities are considered. Results are discussed in detail.

2. Finite Element Model of the Bridge

2.1. Description of the bridge

The bridge is located in Haydarpaşa-Eskişehir railway line at 235+470 km and built at 1980. There are 7 steel truss spans on the bridge. The multi-span truss girder bridge is supported by abutments at the edges and 6 piers at the middle spans. One edge of steel truss span is simply supported, and the other edge is designed as sliding support on rollers and length of a span is 25.7m while total length of the bridge is 187 m. The bridge has a 300 m curve radius. Steel girders on spans are composed of angle section, IPN, UPN hot-rolled sections, steel plates and built-up sections. The bridge is a deck-type truss bridge. The old and new conditions, of the bridge are shown in Fig. 1.

2.2. Finite element model of the bridge

Commercial finite element software to be used to model the 3D bridge. All the elements of the bridge were modeled by 2-node beam element according to the shop drawings and site visual inspections. Computer model was developed by including elements, supports, all irregularities and their connections to each other. Due to centerline differences of the connected beam members, eccentricity at the connection points was taken into account during modeling of the bridge. The weight of the sleepers, ballast, and rails were applied to the dead load at the appropriate nodes. Bridges have 40cm ballast under sleepers. Steel material of the bridge was used as St 37 given in the project. Elastic modulus of the masonry piers was taken as 28 GPa.

Fig. 1. General views of the Bekdemir railway bridge.

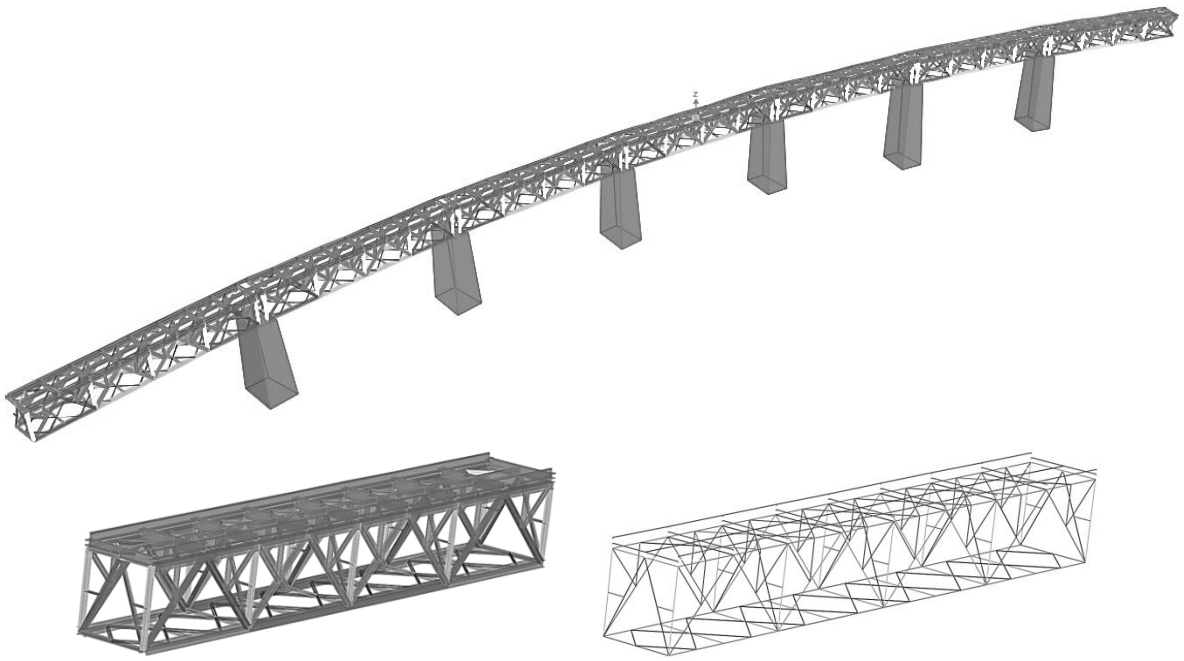

Fig. 2. Finite element model of the Bekdemir bridge.

3D model of the bridge includes 1471 points, 2054 frame elements, and 276 link elements. 16 uni-axial accelerometers were used to measure accelerations of the bridge caused by the passage of test vehicle. The accelerometers were attached to a heavy steel angle base having three short adjustable pointed legs, so that the combined unit, when placed without any attachments and easy to level, would pick up the bridge accelerations. Mode shapes and modal frequencies of the bridge model were compared with the mode shapes and frequencies that were calculated by processing the field test acceleration signals and 3D model of the bridge was updated. Frequencies of first longitudinal and transverse directions are calculated as 3.92s and 5.15s, respectively. Nonlinear time history analyses were conducted using selected earthquake data. Also, both material and geometric nonlinearity were considered in the analysis. Piers were defined as a linear elastic element. Concentrated plastic hinge approach was used to define the nonlinear behavior of the material. SAP2000 (2017) PMM plastic hinge acceptance which is given FEMA 356 Equation 5-4 was used to define the plastic joints of the bridge elements. Mode shape and modal frequency of bridge model are compared with the field test results and 3D model of bridge is updated.

3. Selection of the Earthquake Record

There are different methods that can be used to determine the demand of a structural system under a seismic effect. Linear static analysis, nonlinear pushover analysis, nonlinear time history analysis and incremental dynamic analysis are some of them. Nonlinear time history analysis needs expensive computational effort in terms of time and money, but gives the most realistic result. So nonlinear time history analysis is commonly used (Özgür, 2009; Choi and Jeon, 2003; Shinozuka et al., 2000a).

Earthquake data were selected by considering different soil types, moment magnitude (4.9-7.4), PGAs (0.001-0.82 g), and epicentral distances from earthquake epicenter (2.5-217.4 km). Fig. 3 shows the distribution of moment with central distance. Sixty real earthquake data were selected for soil types A, B, and C, and unscaled earthquake data were used for time history analysis.

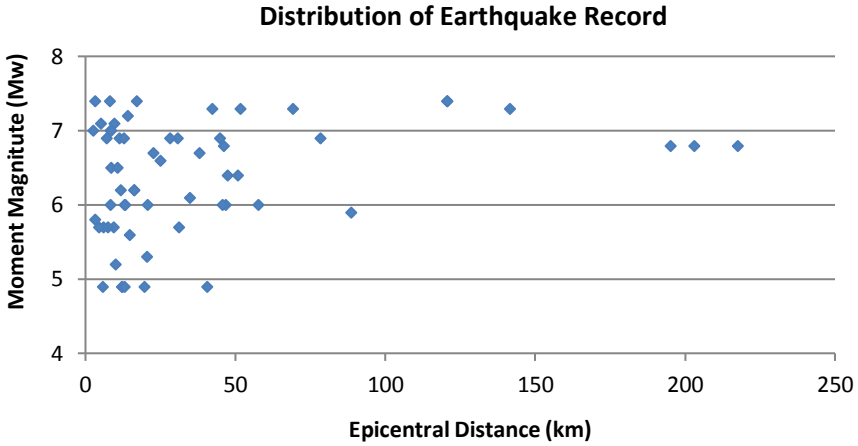

Fig. 3. Distribution of earthquake record in terms of epicentral distance and moment magnitude.

4. Fragility Curve

4.1. Probabilistic seismic demand model

Probabilistic seismic demand model (PSDMs) defines the structural demand in terms of intensity measure (IMs). Seismic performance of a structural and nonstructural member can be calculated by using PSDMs (Choi et al., 2004). Eq. (1) can be used to derive PSDMs.

$$P[EDP \geq d|IM] = 1 - \theta\left(\frac{ln(d) - ln(E\widehat{D}P)}{\beta_{EDP|IM}}\right), \quad (1)$$

where, θ is standard normal distribution function, $E\widehat{D}P$ is the median value of engineering demand, d is the limit state to determine damage level and $\beta_{EDP|IM}$ (dispersion) is the conditional standard deviation of the regression. $E\widehat{D}P$ can be estimated by Eq. (2). Eq. (3) is obtained in linear form if the two sides of Eq. (2) are taken as *ln*. $\beta_{EDP|IM}$ can be calculated using Eq. (4) while a and b are regression coefficients.

$$E\widehat{D}P = aIM^b, \quad (2)$$

$$ln(EDP) = ln(a) + bln(IM), \quad (3)$$

$$\beta_{EDP|IM} \cong \sqrt{\frac{\sum\left(ln(d_i) - ln\left(aIM^b\right)\right)^2}{N-2}}. \quad (4)$$

4.2. Determining serviceability limit state

During the usage period, different damages and displacements of the bridge elements have been observed. However, there are also some geometrical features that the bridges must have so that the railway line can be safely used. In EN 1990 Annex 2 (2001), lateral displacement limits of bridges are defined separately for three different train speeds, for single span and multi-span bridges as can be seen in Table 1.

Table 1. EN 1990 Annex 2 (2001) lateral displacement limits.

Speed Rating V (km/h)	Single Span	Multi-Span
	Radius (1/m)	Radius (1/m)
$V \leq 120$	1700	3500
$120 < V \leq 200$	6000	9500
$V > 200$	14000	17500

This study considered the lateral displacement limits state in EN 1990 Annex 2 (2001) and derived fragility curve to determine whether the displacement limits were exceeded under earthquake motion or not. Trainloads were not considered while nonlinear time history analyses were running and lateral displacements were recording.

4.3. Derivation of the fragility curve

Mid-span displacements gathered from 60 nonlinear time history analyses were used to derive a probabilistic seismic demand model (PSDMs). PGA was used as an intensity measure (IMs). By using PSDMs lateral displacement of bridge at mid-span points were determined in terms of IMs. For the nonlinear time history analysis runs, earthquake records were applied to all bridge piers and edge supports simultaneously and equally. Lateral displacement obtained at the mid-span of the bridge could also be affected by the displacements between the bridge piers, by the curvature of bridge geometry and by the differences of bridge piers foundation's soil condition. Therefore the assumptions made during the analysis should be studied carefully while the PSDMs is being developed, and fragility curve is being used.

Fig. 4 shows PSDMs of mid-span displacements of the bridge. PSDMs can be defined based on Eq. (2) by using a power function of IMs and Eq. (3) by regarding the linear function of IMs. Regression coefficients a and b are shown in Fig. 4. b value shows the correlation between the EDP and IMs. The highest value of b shows more correlated IMs and EDP (Padgett et al., 2008).

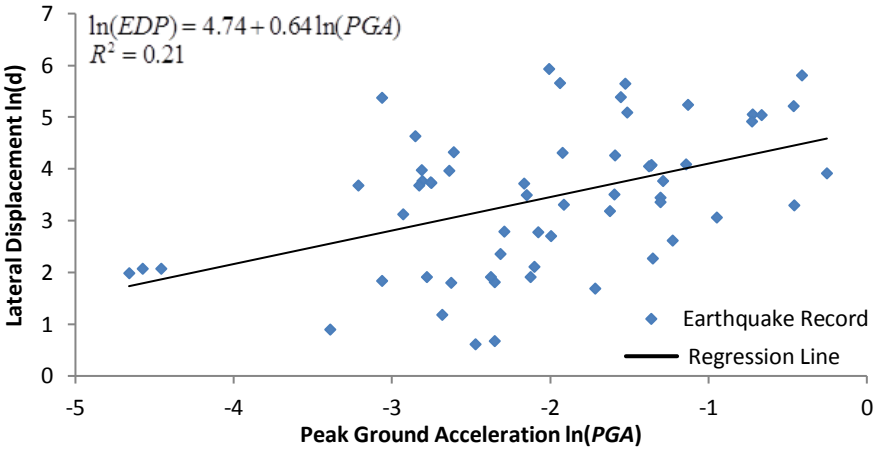

Fig. 4. Probabilistic seismic demand model.

Fragility curves of the bridge were derived considering both single span and multi-span condition. There was limited lateral displacements at the top of the bridge piers, because, the rigidity of the piers. Therefore lateral displacements recorded in the middle of the first span and fourth span were close to each other.

Fig. 5 shows the Fragility curve of the bridge in term of serviceability limit state. Fragility curves were derived for three different velocities that were V<120 km/h, 120 km/h<V<200 km/h and 200 km/h<V, respectively For the Bekdemir bridge %50 probability of exceeding the serviceability limits occured for V>200 km/h at PGA=0.1g for 120<V<200 km/h at PGA=0.175g and for V<120 at PGA=0.475g, respectively.

5. Conclusions

In this study, the earthquake performance of a multi-span steel railway bridge on the Istanbul-Ankara railway line, which is still in service, was determined with the help of fragility curves. Finite element model of the bridge was constructed, and nonlinear time history analyses were carried out for the bridge under the effect of selected 60 different real earthquake data. Relation between the lateral displacements, obtained for the mid-point of the girder bridge spans and IMs were determined by PSDMs. Multi-span lateral displacement limit states specified in EN 1990 Annex 2 were used to derive fragility curves. The PGA values were determined, which

resulted in exceeding the boundary condition with %50 probability for multi-span fragility curve. It was seen that the bridge could exceed the limit considered for the serviceability conditions even in the case of small intensity measures. Moreover, the increase of the train speed enhanced the possibility of the bridge exceeding the damage limit state. In the direction of this study, it is suggested that train speeds needs to be limited to the related multi-span steel truss bridge. As a consequence, for the same type bridges, the speed is a limitation consideration that must be taken into account by the local authorities.

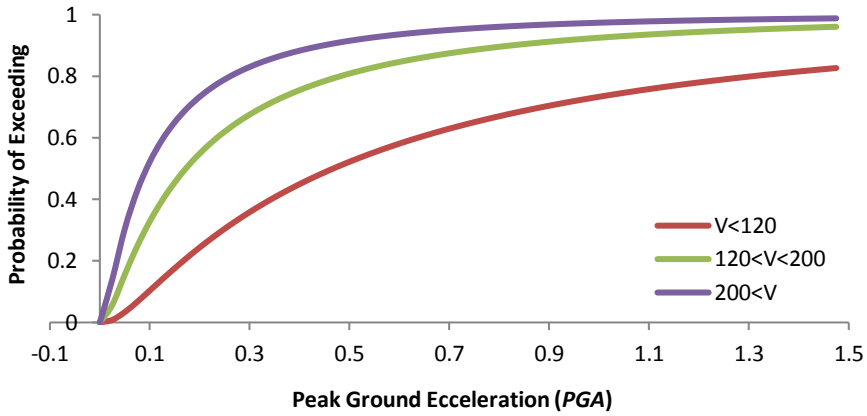

Fig. 5. Multi-span bridge serviceability fragility curve.

Acknowledgements

This research presented in this paper was supported by the TCDD and TUBİTAK 114M332 project. Any opinions expressed are those of authors and do not reflect the opinions of the supporting agencies.

References

Banerjee S, Shinozuka M (2007). Nonlinear static procedure for seismic vulnerability assessment of bridges. *Computer-Aided Civil and Infrastructure Engineering*, 22(4), 293–305.

Bignell JL, LaFave JM, Wilkey JP, Hawkins NM (2004). Seismic evaluation of vulnerable highway bridges with wall piers on emergency routes in Southern Illinois. *13th World Conference on Earthquake Engineering*, Vancouver, Canada.

Choi E, Jeon JC (2003). Seismic fragility of typical bridges in moderate seismic zones. *KSCE Journal of Civil Engineering*, 7(1), 41–51.

Choi E, DesRoches R, Nielson B (2004). Seismic fragility of typical bridges in moderate seismic zones. *Engineering Structures*, 26(2), 187–199.

Çağlıyan A, Yıldız AB (2013). Türkiye'de demiryolu güzergahları jeomorfoloji ilişkisi (Turkey association of railway routes-Geomorphology). *Marmara Coğrafya Dergisi*, 28, 466–486.

EN1990-prANNEX A2. (2001). Eurocode: Basis of Structural Design, Annex2: Application for bridges design. European Committee for Standardization, Brussels, Belgium.

Kumar R, Gardoni P (2014). Effect of seismic degradation on the fragility of reinforced concrete bridges. *Engineering Structures*, 79, 267–275.

Mackie K, Stojadinovic B (2003). Seismic demands for performance-based design of bridges. PEER Report 2003/16, University of California, Berkeley, California, USA.

Mackie K, Stojadinovic B (2001). Probabilistic Seismic Demand Model for California Highway Bridges. *ASCE Journal of Bridge Engineering*, 6(6), 468–481.

Nielson B G (2005). Analytical Fragility Curves for Highway Bridges in Moderate Seismic Zones. *Ph.D. thesis*. Georgia Institute of Technology, Atlanta, USA.

Özgür A (2009). Fragility Based Seismic Vulnerability Assessment of Ordinary Highway Bridges in Turkey. *Ph.D. thesis*. Middle East Technical University, Ankara, Turkey.

Padgett JE, Nielson B G, DesRoches R (2008). Selection of optimal intensity measures in probabilistic seismic demand models of highway bridge portfolios. *Earthquake Engineering & Structural Dynamics*, 37(5), 711–725.

Pan Y, Agrawal AK, Ghosn M, Alampalli S (2010a). Seismic fragility of multispan simply supported steel highway bridges in New York State. I: bridge modeling, parametric analysis, and retrofit design. *ASCE Journal of Bridge Engineering*, 15(5), 448-461.

Pan Y, Agrawal AK, Ghosn M, Alampalli S (2010b). Seismic fragility of multispan simply supported steel highway bridges in New York State. II: fragility analysis, fragility curves, and fragility surfaces. *ASCE Journal of Bridge Engineering*, 15(5), 462-472.

SAP2000 V19. (2017). Integrated finite element analysis and design of structures basic analysis reference manual. Computers and Structures Inc., Berkeley, California, USA.

Shinozuka M, Banerjee S, Kim SH (2007a). Fragility considerations in highway bridge design. Technical Report MCEER-07-0023, University at Buffalo, New York, USA.

Shinozuka M, Banerjee S, Kim SH (2007b). Statistical and mechanistic fragility analysis of concrete bridges. Technical Report MCEER-07-0015, University at Buffalo, New York, USA.

Shinozuka M, Feng M Q, Lee J, Naganuma T (2000a). Statistical analysis of fragility curves. *ASCE Journal of Engineering Mechanics*, 126(12), 1224–1231.

Shinozuka M, Feng MQ, Kim HK, Kim SH (2000b). Nonlineer static procedure for fragility curve development. *ASCE Journal of Engineering Mechanics*, 126(12), 1287–1295.

Challenge Journal of Structural Mechanics

Research Article

Forced vibration analysis of Mindlin plates resting on Winkler foundation

Yaprak I. Özdemir *

Department of Civil Engineering, Karadeniz Technical University, 61080 Trabzon, Turkey

ABSTRACT

The purpose of this paper is to study shear locking-free parametric earthquake analysis of thick and thin plates resting on Winkler foundation using Mindlin's theory, to determine the effects of the thickness/span ratio, the aspect ratio and the boundary conditions on the linear responses of thick and thin plates subjected to earthquake excitations. In the analysis, finite element method is used for spatial integration and the Newmark-β method is used for the time integration. Finite element formulation of the equations of the thick plate theory is derived by using higher order displacement shape functions. A computer program using finite element method is coded in C++ to analyze the plates clamped or simply supported along all four edges. In the analysis, 8-noded finite element is used. Graphs are presented that should help engineers in the design of thick plates subjected to earthquake excitations. It is concluded that 8-noded finite element can be effectively used in the earthquake analysis of thick plates. It is also concluded that, in general, the changes in the thickness/span ratio are more effective on the maximum responses considered in this study than the changes in the aspect ratio.

ARTICLE INFO

Article history:
Received 22 December 2017
Revised 24 January 2018
Accepted 1 February 2018

Keywords:
Earthquake analysis
Thick plate
Mindlin's theory
8-noded finite element
Winkler foundation

1. Introduction

The plates resting on elastic foundation is one of the most popular topics for the last decade in many engineering application. Winkler model, Pasternak model, Hetenyi model, Vlasov and Leont'ev model are the models used by the researchers to calculate the soil effects on the plate.

Winkler model is used as a set of uncorrelated elastic springs attached to each node of the plate (Winkler, 1867). In this method, the deflections are only related with the load on the plate. The deflection of neighbouring points of the foundation is independent of each other. Hetenyi (1950) proposed a two-parameter model, Pasternak model takes in to account the effects of shear interaction among joining points in the foundation (Pasternak, 1957). Vlasov and Leont'ev (1989) related the solution with a γ parameter which is calculated with soil material and thickness of the soil.

The dynamic behavior of thick elastic plates has been investigated by many researchers (Timoshenko and Krieger, 1959; Leissa, 1973; Ugural, 1981; Providakis and Beskos, 1989a, 1989b; Qiu and Feng, 2000; Grice and Pinnington, 2002; Lok and Cheng, 2001; Si et al., 2005; Wu, 2012; Kutlu et al., 2012; Sheikholeslami and Saidi, 2013; Tahouneh 2014 Benferhat et al., 2016; Zamani et al., 2017; Senjanovic et al., 2017). Ayvaz et al. (1998) derived the equations of motions for thick orthotropic elastic plates using Hamilton's principle, but did not present any results. Omurtag and Kadıoğlu (1998) are studied free vibration analysis of orthotropic plates resting on Pasternak foundation by mixed finite element formulation, Ayvaz and Oguzhan (2008) are analysis free vibration of thick plates resting on Vlasov elastic foundation. Ozgan and Daloğlu (2012) are analysis free vibration of thick plates resting on Winkler elastic foundation. All these studies are use 4- and 8-noded finite element which are second and third ordered mathematically.

* *Corresponding author*. Tel.: +90-462-3774018 ; E-mail address: yozdemir@ktu.edu.tr (Y. I. Özdemir)
ISSN: 2149-8024 / DOI: https://doi.org/10.20528/cjsmec.2018.01.004

These elements are known having shear locking problem. Thick plates have a shear locking problem (Zienkiewicz and Taylor, 2000) while the thickness becomes smaller. This means that the bending energy, which should dominate the shear terms, will be incorrectly estimated to be zero in thin plate problems. Shear locking can be avoided by increasing the mesh size, i.e. using finer mesh, but if the thickness/span ratio is "too small", convergence may not be achieved even if the finer mesh is used for the first and second order displacement shape functions. Either refining the finite-element mesh or increasing the order of the shape functions can improve the accuracy of finite-element solutions. The former is called h-version and the latter p-version. It is well known that p convergence is more rapid than h convergence using the same number of degrees of freedom (DOFs) (Zienkiewicz and Taylor, 1989). These problems can be prevented with using true shape function while built up the mathematical model.

The purpose of this paper is to study parametric earthquake analysis of thick plates resting on Winkler foundation, to determine the effects of the thickness/span ratio, the aspect ratio and the boundary conditions on the linear responses of the thick plates subjected to earthquake excitations. A computer program using finite element method is coded in C++ to analyse the plates clamped or simply supported along all four edges. In the program, the finite element method is used for spatial integration and the Newmark-β method is used for the time integration. Finite element formulation of the equations of the thick plate theory is derived by using second order displacement shape functions. In the analysis, 8-noded finite element is used to construct the stiffness and mass matrices.

2. Mathematical Model

The governing equation for a flexural plate (Fig. 1) subjected to an earthquake excitation without damping can be given as (Ayvaz et al., 1998; Tedesco et al., 1999);

$$[M]\{\ddot{w}\}+[K]\{w\}=[F]=-[M]\{\ddot{u}_g\}, \tag{1}$$

where [K] and [M] are the stiffness matrix and the mass matrix of the plate, respectively, w and $\ddot{w}_g$ are the lateral displacement and the second derivative of the lateral displacement of the plate with respect to time, respectively, $\ddot{u}_g$ is the earthquake acceleration.

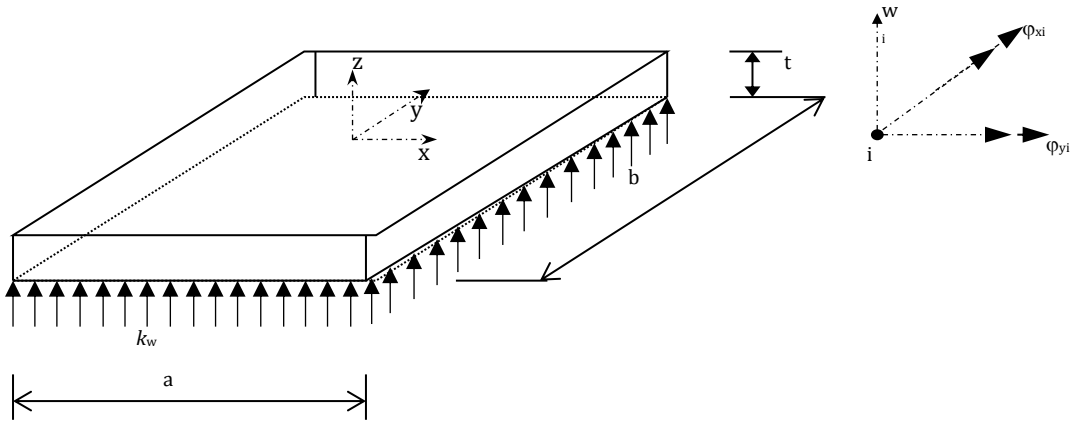

Fig. 1. The sample plate used in this study.

In order to do forced vibration analysis of a plate, the stiffness, [K], mass matrices, [M], and equivalent nodal loads vector, [F], of the plate should be constructed. The evaluation of these matrices is given in the following sections.

The total strain energy of plate-soil-structure system (see Fig. 1) can be written as;

$$\Pi = \Pi_p + \Pi_s + V, \tag{2}$$

where Π_p is the strain energy in the plate,

$$\prod_p = \frac{1}{2}\int_A \left(-\frac{\partial\varphi_x}{\partial x} \quad \frac{\partial\varphi_y}{\partial y} \quad -\frac{\partial\varphi_x}{\partial y}+\frac{\partial\varphi_y}{\partial x}\right)^T E_\kappa \left(-\frac{\partial\varphi_x}{\partial x} \quad \frac{\partial\varphi_y}{\partial y} \quad -\frac{\partial\varphi_x}{\partial y}+\frac{\partial\varphi_y}{\partial x}\right) d_A$$

$$+\frac{k}{2}\int_A \left(-\varphi_x+\frac{\partial w}{\partial x} \quad \varphi_y+\frac{\partial w}{\partial y}\right)^T E_\gamma \left(-\varphi_x+\frac{\partial w}{\partial x} \quad \varphi_y+\frac{\partial w}{\partial y}\right) d_A, \tag{3}$$

where Πs is the strain energy stored in the soil;

$$\prod_s = \frac{1}{2}\int_0^H \int_{-\infty}^{\infty}\int_{-\infty}^{\infty} \sigma_{ij}\varepsilon_{ij} \ , \tag{4}$$

and V is the potential energy of the earthquake loading;

$$V=-\int_A \bar{q} w d_A \ . \tag{5}$$

In this equation E_κ and E_γ are the elasticity matrix and these matrices are given below at Eq. (14), $\bar{q}$ shows earthquake loading.

2.1. Evaluation of the stiffness matrix

The total strain energy of the plate-soil system according to Eq. (2) is;

$$U_e = \frac{1}{2}\int_A \left(-\frac{\partial\varphi_x}{\partial x} \quad \frac{\partial\varphi_y}{\partial y} \quad -\frac{\partial\varphi_x}{\partial y}+\frac{\partial\varphi_y}{\partial x}\right)^T E_\kappa \left(-\frac{\partial\varphi_x}{\partial x} \quad \frac{\partial\varphi_y}{\partial y} \quad -\frac{\partial\varphi_x}{\partial y}+\frac{\partial\varphi_y}{\partial x}\right) d_A$$

$$+\frac{k}{2}\int_A \left(-\varphi_x+\frac{\partial w}{\partial x} \quad \varphi_y+\frac{\partial w}{\partial y}\right)^T E\gamma \left(-\varphi_x+\frac{\partial w}{\partial x} \quad \varphi_y+\frac{\partial w}{\partial y}\right) d_A + \frac{1}{2}\int_A (w_{x,y})^T \mathrm{K}(w_{x,y}) d_A \ . \tag{6}$$

At this equation the first and second part gives the conventional element stiffness matrix of the plate, $[k_p^e]$, differentiation of the third integral with respect to the nodal parameters yields a matrix, $[k_w^e]$, which accounts for the axial strain effect in the soil. Thus the total energy of the plate-soil system can be written as;

$$U_e = \frac{1}{2}\{w_e\}^T \left(\left[k_p^e\right]+\left[k_w^e\right]\right)\{w_e\} d_A \ , \tag{7}$$

where

$$\{w_e\} = \left[w_1 \quad \varphi_{y1} \quad \varphi_{x1} \quad \ldots \quad w_n \quad \varphi_{yn} \quad \varphi_{xn}\right]^T \ . \tag{8}$$

Assuming that in the plate of Fig. 1 u and v are proportional to z and that w is the independent of z (Mindlin, 1951), one can write the plate displacement at an arbitrary x, y, z in terms of the two slopes and a displacement as follows;

$$\{w, v, u\} = \{w_0(x,y,t),\ z\varphi_y(x,y,t),\ -z\varphi_x(x,y,t)\}, \tag{9}$$

where w_0 is average displacement of the plate, and φ_x and φ_y are the bending slopes in the x and y directions, respectively.

The nodal displacements for 8-noded quadrilateral serendipity element (MT8) (Fig. 2) can be written as follows;

$$u = z\varphi_x = -z\sum_{i=1}^{8} h_i \varphi_{xi} \ ,$$

$$v = z\varphi_y = z\sum_{i=1}^{8} h_i \varphi_{yi} \ ,$$

$$w = \sum_{i=1}^{8} h_i w_i \quad . \tag{10}$$

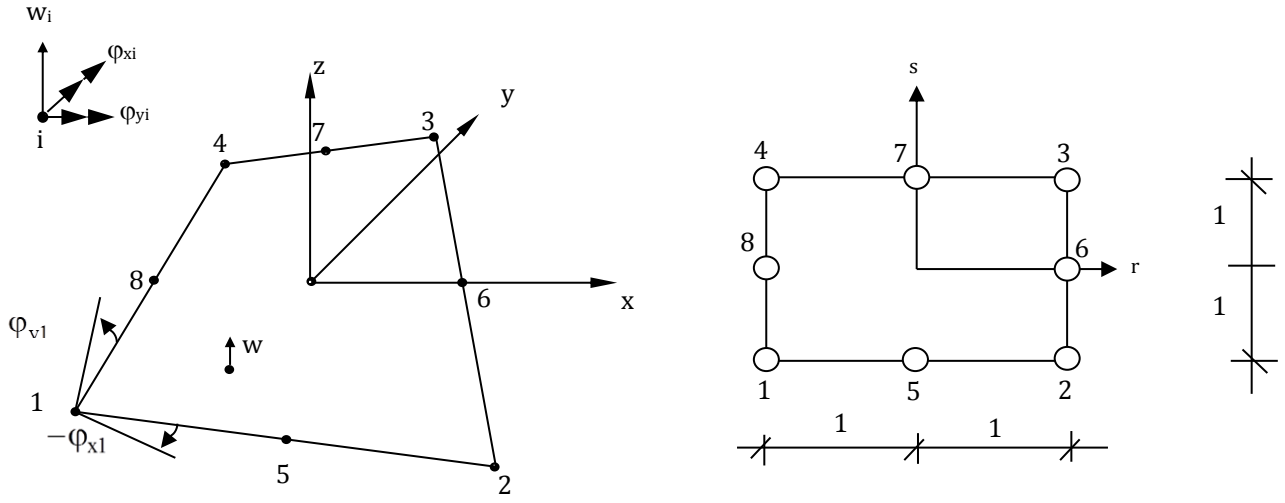

Fig. 2. 8-noded quadrilateral finite element used in this study (Bathe, 1996).

The displacement function chosen for this element is;

$$w = c_1 + c_2 r + c_3 s + c_4 r^2 + c_5 rs + c_6 s^2 + c_7 r^2 s + c_8 rs^2 \ . \tag{11}$$

From this assumption, it is possible to derive the displacement shape function to be;

$$h = [h_1, h_2, h_3, h_4, h_5, h_6, h_7, h_8] \ . \tag{12}$$

Then, the strain-displacement matrix [B] for this element can be written as follows (Cook et al., 1989);

$$[B] = \begin{bmatrix} 0 & 0 & -\frac{\partial h_i}{\partial x} & \ldots \\ 0 & \frac{\partial h_i}{\partial y} & 0 & \ldots \\ 0 & \frac{\partial h_i}{\partial x} & -\frac{\partial h_i}{\partial y} & \ldots \\ \frac{\partial h_i}{\partial x} & 0 & -h_i & \ldots \\ \frac{\partial h_i}{\partial y} & h_i & 0 & \ldots \end{bmatrix}_{5x24} \quad i = 1,\ldots,8 \text{ for } 8\text{-noded element}. \tag{13}$$

The stiffness matrix for MT8 element can be obtained by the following equation [Cook et al., 1989].

$$k_p = \int_V B^T E B dV = \int_V \begin{bmatrix} z\overline{B}_k^T & B_\gamma^T \end{bmatrix} \begin{bmatrix} E_k & 0 \\ 0 & E_\gamma \end{bmatrix} \begin{bmatrix} z\overline{B}_k^T \\ B_\gamma^T \end{bmatrix} dV$$
$$k_p = \int_V \left(z^2 \overline{B}_k^T E_k \overline{B}_k \right) + \left(\overline{B}_\gamma^T E_\gamma \overline{B}_\gamma \right) dV . \quad (14)$$

Integration of Eq. (14) through the thickness yields;

$$k_p = \int_A \left(\overline{B}_k^T \overline{E}_k \overline{B}_k + \overline{B}_\gamma^T \overline{E}_\gamma \overline{B}_\gamma \right) dA , \quad (15)$$

where the first term concerns with the bending and the second term concerns with the shear effects of the thick plate. Thus,

$$k_p = \int_A \overline{B}^T \overline{E} \overline{B} dA = \int_{-1}^{1} \int_{-1}^{1} \overline{B}^T \overline{E} \overline{B} |J| dr ds , \quad (16)$$

which must be evaluated numerically (Bathe, 1996).

2.2. Foundation formulation

As explained before, Winkler model is the simplest model for the plates resting on elastic foundation. In this model, all the deflections on the plate are due to the load on it. The foundation is represented with a set of uncorrelated elastic springs. So in the analysis, the stiffness of these springs are calculated and are added to the element stiffness matrix. The stiffness matrices for the Winkler foundation can be derived by;

$$k_w = k \int_{-1}^{1} \int_{-1}^{1} [h]^T [h] |J| dr ds , \quad (17)$$

where k is the elastic foundation modulus.

After calculating all element stiffness matrices, global stiffness matrix can be assembled as;

$$[\mathrm{K}] = \sum_{i=1}^{p_e} \left([\mathrm{k_p}] + [\mathrm{k_w}] \right) , \quad (18)$$

where p_e is the node number.

2.3. Evaluation of the mass matrix

The formula for the consistent mass matrix of the plate may be written as;

$$M = \int_\Omega H_i^T \mu H_i d\Omega , \quad (19)$$

In this equation, μ is the mass density matrix of the form (Tedesco et al., 1999).

$$\mu = \begin{bmatrix} m_1 & 0 & 0 \\ 0 & m_2 & 0 \\ 0 & 0 & m_3 \end{bmatrix} , \quad (20)$$

where $m_1=\rho_p t$, $m_2=m_3= 1/12\left(\rho_p t^3\right)$, and ρ_p is the mass densities of the plate. And H_i can be written as follows,

$$H_i = \begin{bmatrix} dh_i/dx & dh_i/dy & h_i \end{bmatrix} \qquad i = 1 \ldots 8. \quad (21)$$

It should be noted that the rotation inertia terms are not taken into account. By assembling the element mass matrices obtained, the system mass matrix is obtained.

2.4. Evaluation of equivalent nodal loads vector

Equivalent nodal loads, [F], can be obtained by the following equation.

$$[\mathrm{F}] = \int H_i^T \overline{q} d\Omega . \quad (22)$$

In this equation, H_i can be obtained by Eq. (21), and $\overline{q}$ denotes

$$-[\mathrm{M}] = \{\ddot{u}_g\} . \quad (23)$$

It should be noted that, in this study, the program, MATLAB, is used for the eigenvalue solution of Eq. (1). It should also be noted that, the Newmark-β method is used for the time integration of Eq. (2) by using the average acceleration method.

3. Numerical Examples

3.1. Data for numerical examples

In the light of the results given in references (Özdemir et al., 2007; Özdemir, 2007), the aspect ratios, b/a, of the plate are taken to be 1, 2.0, and 3.0. The thickness/span ratios, t/a, are taken as 0.05, 0.1, 0.2, and 0.3 for each aspect ratio. The shorter span length of the plate is kept constant to be 3 m. The mass density, Poisson's ratio, and the modulus of elasticity of the plate are taken to be 2.5 kN s^2/m^2, 0.2, and 2.7x10^7 kN/m^2. Shear factor k is taken to be 5/6. The subgrade reaction modulus of the Winkler-type foundation is taken to be 5000 kN/m^3.

In order to obtain the response of each plate by using the time history analysis, the East-West component of March 13, 1992 Erzincan earthquake in Turkey is used. Duration of this earthquake is 21 s, but, in this study, the first 8 s of the earthquake is used since the peak value of the record occurred in this range (Fig. 3).

For the sake of accuracy in the results, rather than starting with a set of a finite element mesh size and time increment, the mesh size and time increment required to obtain the desired accuracy were determined before presenting any results This analysis was performed separately for the mesh size and time increment. It was concluded that the results have acceptable error when equally spaced 8x8 mesh sizes are used for a 3 m x 3 m plate even if it is a thin plate, if the 0.01s time increment is used. Length of the elements in the x and y directions are kept constant for different aspect ratios as in the case of square plate.

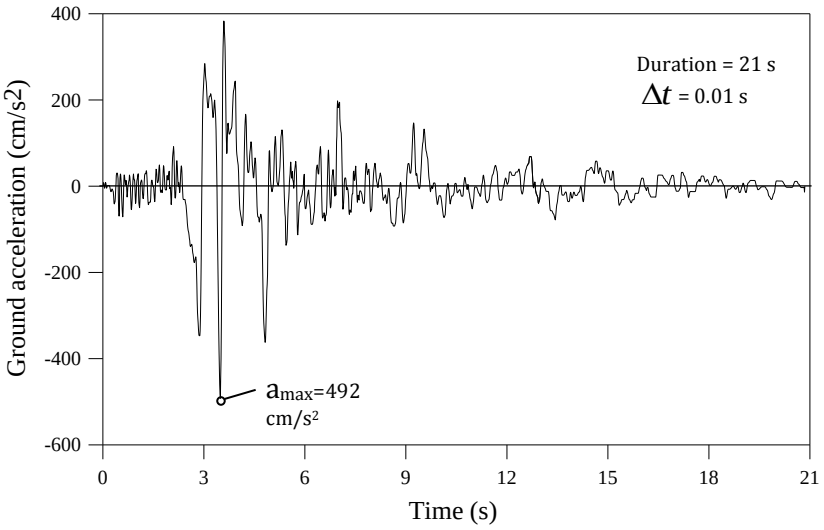

Fig. 3. East-West component of the March 13, 1992 Erzincan earthquake in Turkey.

3.2. Results

One of the purposes of this paper was to determine the time histories of the displacements and the bending moments at different points of the thick plates subjected to earthquake excitations, but presentation of all of the time histories would take up excessive space. Hence, only the absolute maximum displacements and bending moments for different thickness/span ratio and aspect ratio are presented after two time histories are given. This simplification of presenting only the maximum responses is supported by the fact that the maximum values of these quantities are the most important ones for design. These results are presented in graphical rather than in tabular form.

The time histories of the center displacements of the thick clamped plates resting on elastic foundation with the subgrade reaction modulus of the Winkler-type foundation 5000 kN/m^3 for b/a= 1.0, and 2.0 when t/a=0.3 are given in Figs. 4(a) and 4(b), respectively.

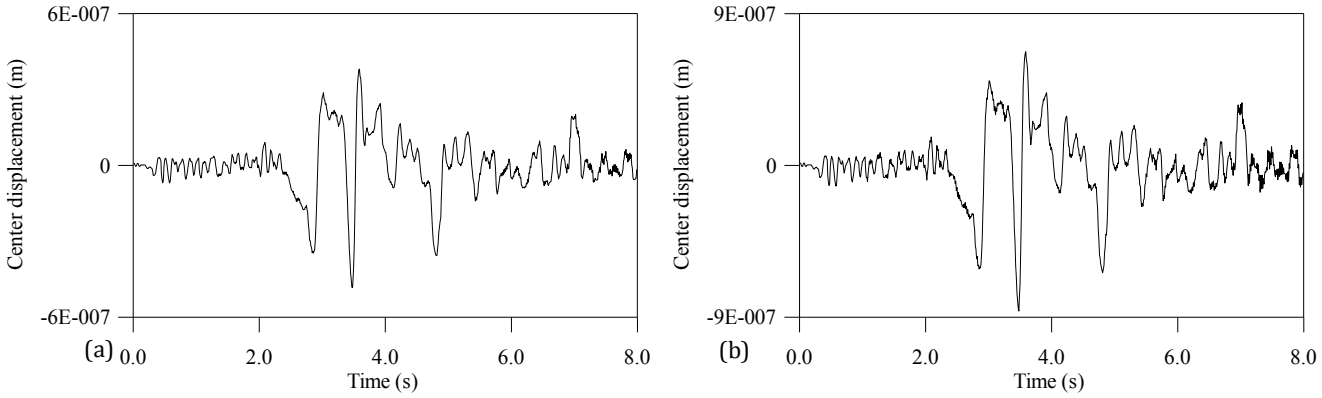

Fig. 4. The time history of the center displacement of the thick clamped plate resting on Winkler foundation for (a) b/a=1.0 and t/a=0.3; (b) b/a=2.0 and t/a=0.3.

As seen from Figs. 4(a) and 4(b), the center displacements of the thick clamped plates for b/a = 1, and t/a = 0.3, and for b/a = 2, and t/a = 0.3, reached their absolute maximum values of 0.000484 mm at 3.48 s, and of 0.000864 mm at 3.48 s, respectively. These absolute maximum values are different even with the same occurring time as the dynamic characteristics of the thick plates affect the response. It is also understandable that the system becomes more flexible as the aspect ratio increases.

The absolute maximum displacements of the thick plates for different aspect ratios, and thickness/span ratios are given in Fig. 5 for the thick plates simply supported along all four edges and in Fig. 6 for the thick plates clamped along all four edges.

As seen from Figs. 5, and 6, the absolute maximum displacements of the thick plates increase with increasing aspect ratio for a constant t/a ratio. The same displacements decrease with increasing t/a ratio for a constant b/a ratio. As also seen from these figures, the decrease in the absolute maximum displacement for a constant b/a ratio increases with increasing b/a ratio. The curves for a constant value of the aspect ratio, b/a are fairly getting closer to each other as the value of

t/a increases. This shows that the curves of the absolute maximum displacements will almost coincide with each other when the value of the thickness/span ratio, t/a, increases more. In other words, the increase in the thickness/span ratio will not affect the absolute maximum displacements after a determined value of t/a.

As also seen from Figs. 5, and 6, the absolute maximum displacements of the thick simply supported plates are larger than those of the thick clamped plates for the same aspect and thickness/span ratios. In general, the effects of the changes in the thickness/span ratios on the absolute maximum displacement are larger than the changes in the aspect ratios.

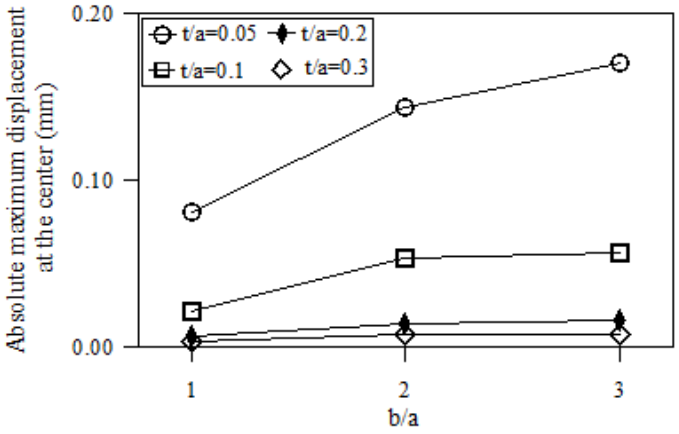

Fig. 5. Absolute maximum displacement of the thick simply supported plates resting on Winkler foundation for different aspect ratios and thickness/span ratios.

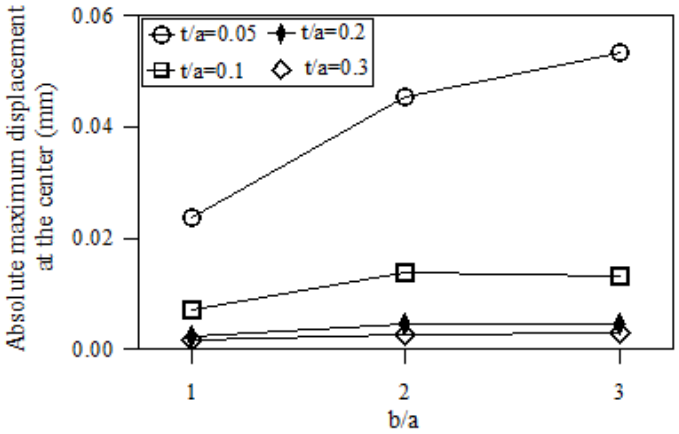

Fig. 6. Absolute maximum displacement of the thick clamped plates resting on Winkler foundation for different aspect ratios and thickness/span ratios.

The absolute maximum bending moments M_x at the center of the thick plates for different aspect ratios and thickness/span ratios are given in Fig. 7 for the thick simply supported plates and in Fig. 8 for the thick clamped plates, respectively.

As seen from Fig. 7, the absolute maximum bending moment, M_x, at the center of the thick simply supported plates increases with increasing aspect ratio and thickness/span ratio. The increases in the absolute maximum bending moment, M_x, increase with increasing aspect and thickness/span ratios. This is understandable that increasing the aspect ratio makes the plate stiffer in the short span, the x axis, direction. As also seen from this figure, in general, the effects of the changes in the aspect ratios on the absolute maximum bending moment, M_x, are larger than the changes in the thickness/span ratios.

As seen from Fig. 8, the absolute maximum bending moment, M_x, at the center of the thick clamped plates, as in the case of the absolute maximum bending moment, M_x, at the center of the thick simply supported plates, increases with increasing aspect ratio and thickness/span ratio. The increases in the absolute maximum bending moment, M_x, increase with increasing aspect and thickness/span ratios. This is also understandable that increasing the aspect ratio makes the plate stiffer in the short span, the x axis, direction. As also seen from this figure, in general, the effects of the changes in the aspect ratios on the absolute maximum bending moment, M_x, are larger than the changes in the thickness/span ratios.

The absolute maximum bending moments M_y at the center of the thick plates for different aspect ratios and thickness/span ratios are given in Fig. 9 for the thick simply supported plates and in Fig. 10 for the thick clamped plates, respectively.

As seen from Fig. 9, the absolute maximum bending moment, M_y, at the center of the thick simply supported plates decreases with increasing aspect ratio and increases with increasing thickness/span ratio. The decrease in the

absolute maximum bending moment, M_y, increase with increasing aspect ratio. The increase in the absolute maximum bending moment, M_y, increases with increasing thickness/span ratios. This is understandable that increasing the aspect ratio makes the thick plates more flexible in the long span, the *y* axis, direction. As also seen from this figure, in general, the effects of the changes in the thickness/span ratios on the absolute maximum bending moment, M_y, are larger than the changes in the aspect ratios.

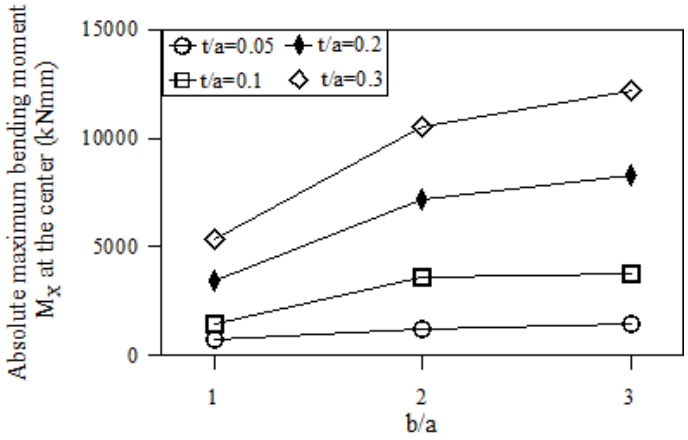

Fig. 7. Absolute maximum bending moment M_x at the center of the thick simply supported plates resting on Winkler foundation for different aspect ratios and thickness/span ratios.

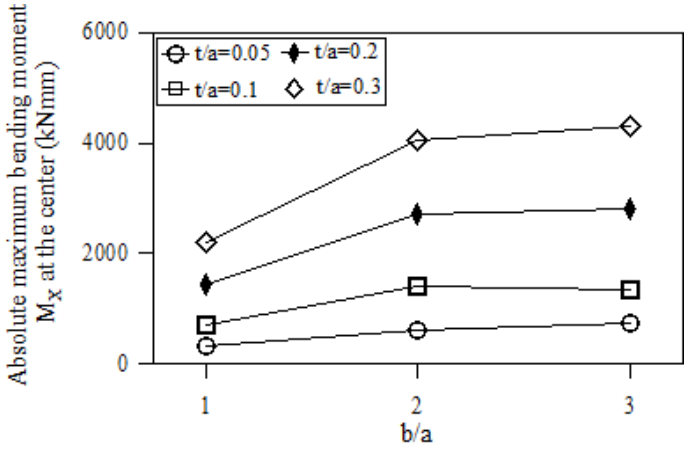

Fig. 8. Absolute maximum bending moment M_x at the center of the thick clamped plates resting on Winkler foundation for different aspect ratios and thickness/span ratios.

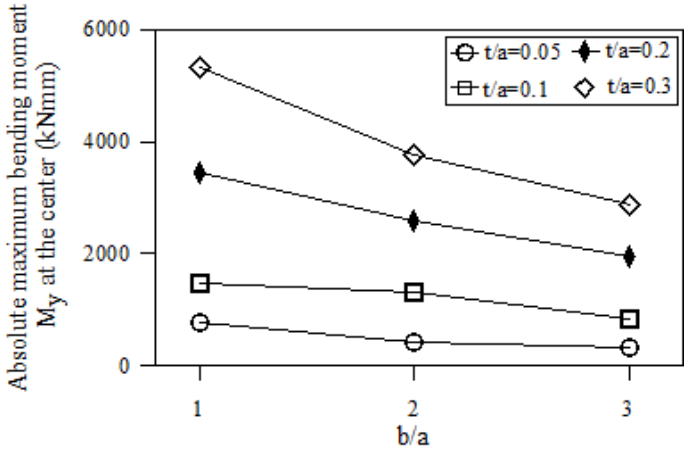

Fig. 9. Absolute maximum bending moment M_y at the center of the thick simply supported plates resting on Winkler foundation for different aspect ratios and thickness/span ratios.

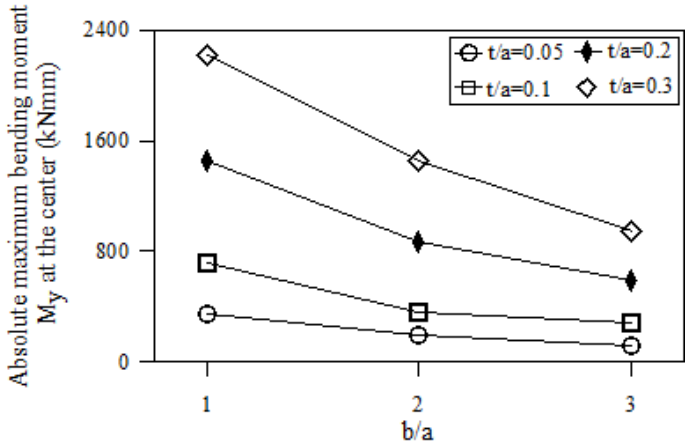

Fig. 10. Absolute maximum bending moment M_y at the center of the thick clamped plates resting on Winkler foundation for different aspect ratios and thickness/span ratios.

As seen from Fig. 10, the absolute maximum bending moment, M_y, at the center of the thick clamped plates, as in the case of the absolute maximum bending moment, M_y, at the center of the thick simply supported plates, decreases with increasing aspect ratio and increases with increasing thickness/span ratio. The decrease in the absolute maximum bending moment, M_y, increase with increasing aspect ratio. The increase in the absolute maximum bending moment, M_y, increases with increasing thickness/span ratios. This is also understandable that increasing the aspect ratio makes the thick plates more flexible in the long span, the y axis, direction. As also seen from this figure, in general, the effects of the changes in the thickness/span ratios on the absolute maximum bending moment, M_y, are larger than the changes in the aspect ratios.

In this study, the absolute maximum bending moments M_x at the center of the edge in the y direction and the maximum bending moment M_y at the center of the edge in the x direction are not presented for the thick plates clamped along all four edges. It should be noted that the variations of these moments are similar to the absolute maximum bending moments M_x at the center of the thick clamped plates.

4. Conclusions

The purpose of this paper is to study shear locking-free parametric earthquake analysis of thick plates resting on Winkler foundation, to determine the effects of the thickness/span ratio, the aspect ratio and the boundary conditions on the linear responses of the thick plates resting on Winkler foundation subjected to earthquake excitations.. It is concluded that 8-noded finite element can be effectively used in the earthquake analysis of thick plates resting on elastic foundation. The coded program can be effectively used in the earthquake analyses of any thick plates resting on elastic foundation. It is also concluded that, in general, the changes in the thickness/span ratio are more effective on the maximum responses considered in this study than the changes in the aspect ratio.

For a thick plates resting on Winkler foundation subjected to the earthquake excitations, it is somewhat difficult to interpret the effects of the thickness/span ratio, the aspect ratio, and the boundary conditions on the responses because both the frequency content of the earthquake excitation and the exact natural frequency of the particular thick plates resting on Winkler foundation can make a difference to its response. In order to generalize the results obtained in this study, the responses of the different thick plates resting on Winkler foundation subjected to different earthquake excitations should be evaluated all together. Therefore, the curves presented herein can help the designer to anticipate the effects of the thickness/span ratio, the aspect ratio, and the boundary conditions on the earthquake response of a thick plate resting on Winkler foundation.

The following conclusions can also be drawn from the results obtained in this study.

- The absolute maximum displacements of the thick plates increase as the aspect ratio increases for a constant t/a ratio. The same displacements decrease as the t/a ratio increases for a constant b/a ratio.
- The changes in the aspect ratios are generally less effective on the absolute maximum displacement than the changes in the thickness/span ratios.
- The absolute maximum bending moment, M_x, at the center of the thick simply supported plates resting on Winkler foundation increases as the aspect ratio and thickness/span ratio increase.
- The changes in the aspect ratios are generally more effective on the absolute maximum bending moment, M_x, of the thick simply supported plates than the changes in the thickness/span ratios.
- The absolute maximum bending moment, M_x, at the center of the thick clamped plates resting on Winkler foundation increases with increasing aspect ratio and thickness/span ratio.
- The changes in the aspect ratios are generally more effective on the absolute maximum bending moment, M_x, of the thick clamped plates resting on Winkler foundation than the changes in the thickness/span ratios.
- The absolute maximum bending moment, M_y, at the center of the thick simply supported plates resting on

Winkler foundation decreases as the aspect ratio increases and increases as the thickness/span ratio increases.

- The changes in the thickness/span ratios are generally more effective on the absolute maximum bending moment, M_y, of the thick simply supported plates resting on Winkler foundation larger than the changes in the aspect ratios.
- The absolute maximum bending moment, M_y, at the center of the thick clamped plates resting on Winkler foundation decreases with increasing aspect ratio and increases with increasing thickness/span ratio.
- The changes in the thickness/span ratios are generally more effective on the absolute maximum bending moment, M_y, of the thick clamped plates resting on Winkler foundation than the changes in the aspect ratios.
- In general, degrees of decreases and increases depend on the changes in the aspect and thickness/span ratios, and the changes in the thickness/span ratio are more effective on the maximum responses considered in this study than the changes in the aspect ratio.

Acknowledgements

This study is supported by the Research Fund of Karadeniz Technical University (Project number: 2002.112.1.5).

References

Ayvaz Y, Daloğlu A, Doğangün A (1998). Application of a modified Vlasov model to earthquake analysis of the plates resting on elastic foundations. *Journal of Sound & Vibration*, 212(3), 499-509.

Ayvaz Y, Oguzhan CB (2008). Free vibration analysis of plates resting on elastic foundations using modified Vlasov model. *Structural Engineering & Mechanics*, 28(6), 635-658.

Bathe KJ (1996). Finite Element Procedures. Prentice Hall, Upper Saddle River, New Jersey.

Benferhat R, Daouadji TH, Mansour MS, Hadji L (2016). Effect of porosity on the bending and free vibration response of functionally graded plates resting on Winkler-Pasternak foundations. *Earthquakes & Structures*, 10(6), 1429-1449.

Cook RD, Malkus, DS, Michael EP (1989). Concepts and Applications of Finite Element Analysis. John Wiley & Sons, Inc., Canada.

Grice RM, Pinnington RJ (2002). Analysis of the flexural vibration of a thin-plate box using a combination of finite element analysis and analytical impedances. *Journal of Sound & Vibration*, 249(3), 499-527.

Hetenyi M (1950). A general solution for the bending of beams on an elastic foundation of arbitrary continuity. *Journal of Applied. Physics,* 21, 55-58.

Kutlu A, Uğurlu B, Omurtag MH (2012). Dynamic response of Mindlin plates resting on arbitrarily orthotropic Pasternak foundation and partially in contact with fluid. *Ocean Engineering,* 42, 112-125.

Leissa AW (1973). The free vibration of rectangular plates. *Journal of Sound & Vibration*, 31(3), 257-294.

Lok TS, Cheng QH (2001). Free and forced vibration of simply supported, orthotropic sandwich panel. *Computers & Structures,* 79(3), 301-312.

Mindlin RD (1951). Influence of rotatory inertia and shear on flexural motions of isotropic, elastic plates. *Journal of Applied Mechanics*, 18, 31-38.

Omurtag MH, Kadıoğlu F (1998). Free vibration analysis of orthotropic plates resting on Pasternak foundation by mixed finite element formulation. *Computers & Structures,* 67, 253-265.

Özdemir YI (2007). Parametric Analysis of Thick Plates Subjected to Earthquake Excitations by Using Mindlin's Theory. *Ph.D. thesis*, Karadeniz Technical University, Trabzon.

Özdemir YI (2012). Development of a higher order finite element on a Winkler foundation. *Finite Element. Analysis and Design,* 48, 1400-1408.

Özdemir YI, Bekiroğlu S, Ayvaz Y (2007). Shear locking-free analysis of thick plates using Mindlin's theory. *Structural Engineering & Mechanics,* 27(3), 311-331.

Özgan K, Daloglu AT (2012). Free vibration analysis of thick plates on elastic foundations using modified Vlasov model with higher order finite elements. *International Journal of Engineering & Materials Sciences*, 19, 279-291.

Pasternak PL (1954). New method of calculation for flexible substructures on two-parameter elastic foundation. Gasudarstvennoe Izdatelstoo. Literatury po Stroitelstvu I Architekture, 1-56, Moscow.

Providakis CP, Beskos DE (1989a). Free and forced vibrations of plates by boundary elements. *Computer Method Applied Mechanics,* 74, 231-250.

Providakis CP, Beskos DE (1989b). Free and forced vibrations of plates by boundary and interior elements. *International Journal of Numerical Methods in Engineering*, 28, 1977-1994.

Qiu J, Feng ZC (2000). Parameter dependence of the impact dynamics of thin plates. *Computers & Structures*, 75(5), 491-506.

Senjanovic I, Tomic M, Hadzic N, Vladimir N (2017). Dynamic finite element formulations for moderately thick plate vibrations based on the modified Mindlin theory. *Engineering Structures,* 136, 100-113.

Sheikholeslami SA, Saidi AR. (2013). Vibration analysis of functionally graded rectangular plates resting on elastic foundation using higher-order shear and normal deformable plate theory. *Computers & Structures,* 106, 350-361.

Si WJ, Lam KY, Gang SW (2005). Vibration analysis of rectangular plates with one or more guided edges via bicubic B-spline method. *Shock & Vibration,* 12(5), 363-376.

Tahouneh V (2014). Free vibration analysis of thick CGFR annular sector plates resting on elastic foundations. *Structural Engineering & Mechanics,* 50(6), 773-796.

Tedesco JW, McDougal WG, Ross CA (1999). Structural Dynamics. Addison Wesley Longman Inc., California.

Timoshenko S, Woinowsky-Krieger S (1959). Theory of Plates and Shells. Second edition, McGraw-Hill, New York.

Ugural AC (1981). Stresses in Plates and Shells. McGraw-Hill, New York.

Vlasov VZ, Leont'ev NN (1989). Beam, plates and shells on elastic foundations. GIFML, Moscow.

Weaver W, Johnston PR (1984). Finite Elements for Structural Analysis. Prentice Hall, Inc., Englewood Cliffs, New Jersey.

Winkler E (1867). Theory of Elasticity and Strength. Dominicus Pague, Czechoslovakia.

Wu LH (2012). Free vibration of arbitrary quadrilateral thick plates with internal colums and uniform elastic edge supports by pb-2 Ritz method. *Structural Engineering & Mechanics,* 44(3), 267-288.

Zamani HA, Aghdam MM, Sadighi M (2017). Free vibration analysis of thick viscoelastic composite plates on visco-Pasternak foundation using higher-order theory. *Computers & Structures,* 182, 25-35.

Zienkiewich OC, Taylor RL, Too JM (1971). Reduced integration technique in general analysis of plates and shells. *International Journal of Numerical Methods in Engineering,* 3, 275-290.

Zienkiewich OC, Taylor RL, Too JM (1989). The Finite Element Method. Fourth ed., McGraw-Hill, New York.

Challenge Journal of Structural Mechanics

Research Article

Investigating the effect of infill walls on steel frame structures

Osman Fatih Bayrak, Seda Yedek, Muhammet Musab Erdem, Murat Bikce *

Department of Civil Engineering, İskenderun Technical University, 31200 Hatay, Turkey

ABSTRACT

Infill walls consisting of materials such as hollow concrete, hollow clay and autoclaved aerated concrete bricks are not only preferred in reinforced concrete buildings but also in steel frame structures. It is a well-known fact that infill walls limit the displacement of frames under horizontal loads. However, they may also bring about certain problems due to being placed randomly in horizontal and discontinuously in vertical directions for some architectural reasons. Moreover, cracks in frame-wall joints are observed in steel frame structures in which ductile behaving steel and brittle behaving infill walls are used together. In this study, the effect of infill walls on steel frames has been investigated. In the steel frame structure chosen for the study, four different situations consisting of different combinations of infill walls have been modeled by using ETABS Software. Later, the pushover analyses have been performed for all the models and their results have been compared. As a result of the analyses done by using the equivalent diagonal strut model, it has been found out that infill walls limit the displacement of steel frames and increase the performance of a structure. However, it has been also determined that in the steel frame structure in which the infill walls have been placed discontinuously in vertical and asymmetrically in horizontal, infill walls may lead to torsional and soft story irregularities. As a result, it is possible to observe cracks in the joints of infill walls and steel frame, the deformation properties of which differ, unless necessary precautions are taken.

ARTICLE INFO

Article history:
Received 11 December 2017
Revised 13 January 2018
Accepted 23 January 2018

Keywords:
Steel structures
Infill walls
Non-structural cracks in elements
Modeling of infill walls

1. Introduction

Infill walls which are widely used in reinforced concrete (RC) buildings are also preferred commonly in steel frame structures for certain architectural reasons. Thus, it is crucial to understand the effect of brittle behaving infill walls between steel frames which show ductile behavior. Infill walls are non-structural elements and they consist of materials such as hollow concrete, clay and autoclaved aerated concrete (AAC) bricks whose raw materials are aggregate, pumice, clay, basaltic pumice, cement, lime and gypsum. Therefore, the effect of infill walls on the structural behavior is ignored and they are only taken into account as dead load in analyses. However, analytical and experimental studies have revealed that infill walls decrease story drift against horizontal loads, provide strength and stiffness to a structure, and thus all this effect cannot be ignored (Kaplan, 2008; İrtem et al., 2005; Beklen and Çağatay, 2009; Sevil et al., 2010; Beklen, 2009; Mehrabi et al., 1996; Murty and Jain, 2000). Yet, along with the contributions of infill walls stated above, there are also other studies available showings that they affect the behavior of a structure in a negative way (Akkuzu, 2007; Yadollahi et al., 2016). The design choices, such as using infill walls only in one axis of a structure, changing the area and position between stories of infill walls (Figs. 1a-b), forming ribbon windows (Figs. 1c-d), might cause torsion, soft story and formation of short column. As a result of the brittle structure of infill wall materials, the compressive stress formed in the corners leads to crushing and local loss of strength. Fig. 2 demonstrates that when the infill walls of the structure whose basement is surrounded with window walls from two sides and with infill walls from the other two sides have been analyzed, torsion in the structure has been determined (Doğan and Bakırcı Er, 2011).

* *Corresponding author*. Tel.: +90-326-6135600 ; Fax: +90-326-6135613 ; E-mail address: murat.bikce@iste.edu.tr (M. Bikce)
ISSN: 2149-8024 / DOI: https://doi.org/10.20528/cjsmec.2018.01.005

While such vertical discontinuity of infill walls increases the stiffness of frames on upper stories, it may lead to excessive stress in structural elements of the basement (Tabeshpour et al., 2012; Murty and Jain, 2000; Anıl and Altın, 2007).

The number of steel structures has been increasing by the reason of its ductile behavior, energy absorbing capacity, fast manufacture, and its being recyclable, environment-friendly and light. They are also economical systems considering that they do not require formwork and scaffolding, they weigh much less, and they can be built in any weather and in less time. In steel frame systems, various partition systems are used in order to meet the need of partitions in the structure (Fig. 3).

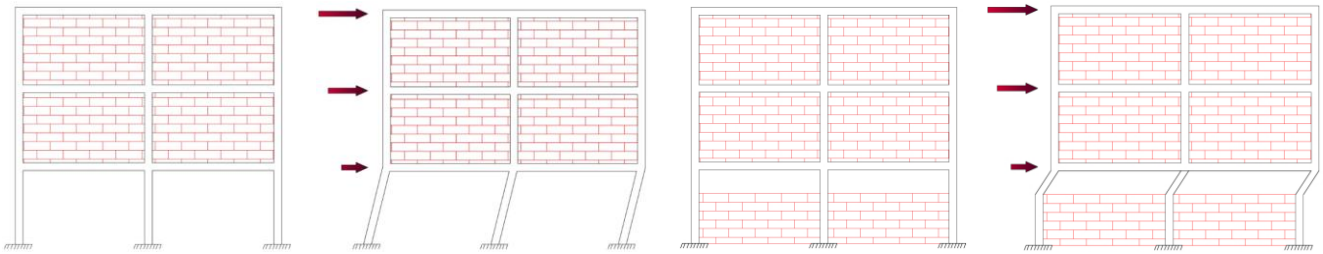

(a) (b) (c) (d)

Fig. 1. (a) The basement of the structure without infill walls; (b) The behavior of the structure without infill at basement under horizontal load; (c) Ribbon window; (d) The formation of short column under horizontal load.

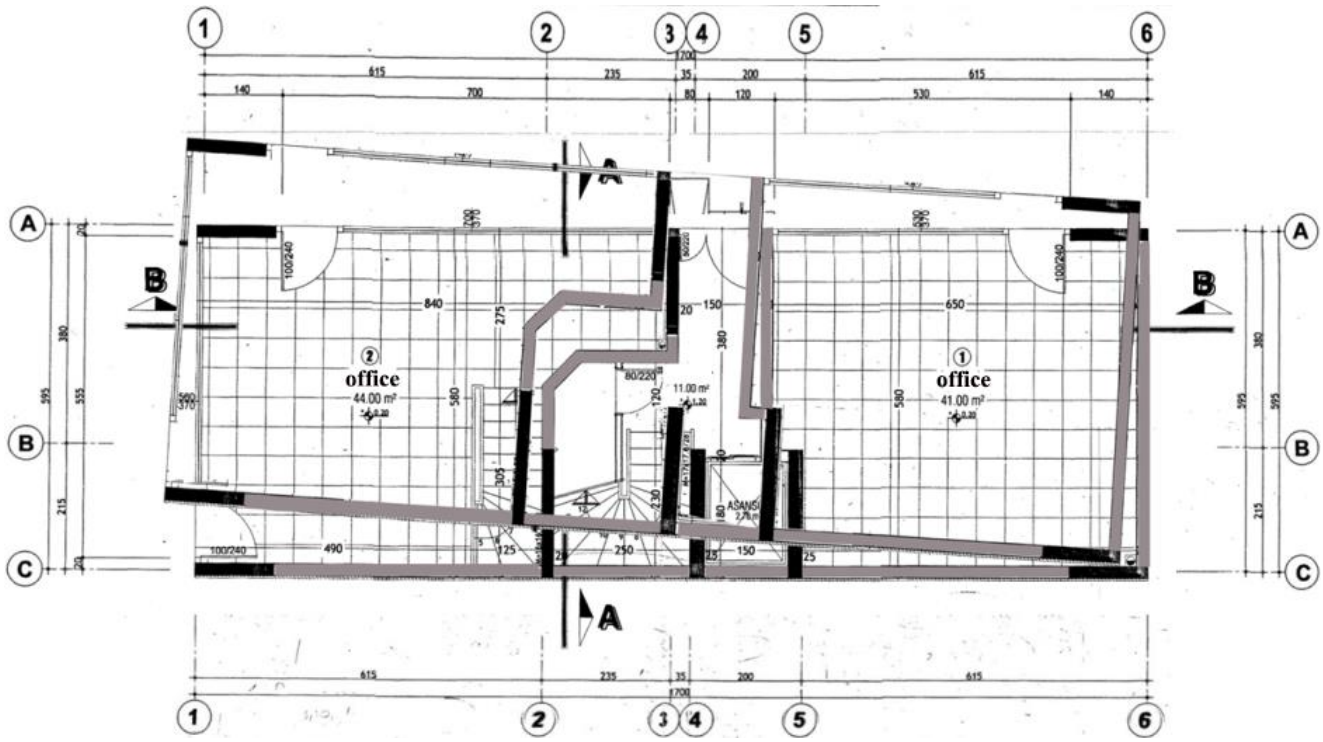

Fig. 2. Basement plan and possible torsion.

(a) (b) (c) (d)

Fig. 3. Steel frame infills: (a) Light section steel and panel; (b) Hollow concrete brick; (c) AAC; (d) Hollow clay brick.

Similar to RC buildings, hollow concrete brick, hollow clay bricks and AAC are used as infill wall material in steel structures. In the experimental studies investigating the effect of infill walls on steel frame systems, as it is in RC buildings, infill walls have been found to increase the horizontal load bearing capacity, lateral stiffness and energy absorbing capacity of the frame system significantly (Kaltakcı et al., 2006; Ghaffarzadeh and Ghalghachi, 2009; Kaymak and Tuna, 2012). However, in almost all these studies, the asymmetrical structure and discontinuity of the infill walls have not been taken into account, yet they have been considered as single span planar frames. Whereas, the behavior of steel structure frames, which are more ductile compared to RC, should be taken into account as three-dimensional with their brittle behaving infill walls. It has been asserted that using steel and infill walls together, which have different mechanical properties, causes cracks in joints (Öktem, 2003). Similarly in Fig. 4, cracks can be seen between the steel frame and the infill wall in finished and unfinished structures. In this study, analyses on a steel structure have been carried out by forming various combinations with infill walls. The effect of infill walls on the structure has been reflected by modeling them with diagonal bars.

Fig. 4. Steel structure under construction and cracks between infill walls and steel frames.

2. The Steel Frame Examined and the Modellings

The steel frame chosen can be seen in Fig. 5a. This frame without infill has been defined as Type 1. Type 2-4, which have been examined to understand asymmetrical effect of infill walls horizontally and vertically, are presented in Fig. 5b-d respectively.

The columns and beams of the steel frame that has been examined are made of an IPE300 steel profile (Fig. 6), and the AAC properties of infill walls are presented in Table 1.

It should not be forgotten that these parameters affect the elasticity module of infill walls and the in-frame strength of infill walls showing different characteristics everywhere cannot be the same, either. Infill walls generate pressure in the column-beam joint region of frame under horizontal loads (Fig. 7). Behavior of infills formulated according to this approach is presented in Eqs. (1) to (3) (FEMA-356, 2000).

$$d = \sqrt{H^2 + L^2}\,, \tag{1}$$

$$W_{ef} = 0{,}175 \times (\lambda \times H)^{-0{,}4} \times d\,, \tag{2}$$

$$\lambda = \sqrt[4]{\frac{E_m \times t \times sin2\theta}{4 \times E_s \times I_c \times h}}\,, \tag{3}$$

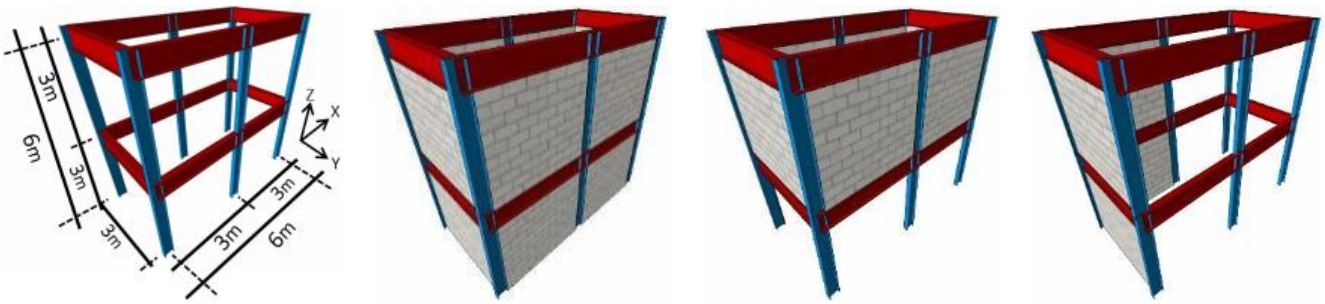

(a) (b) (c) (d)

Fig. 5. Steel frames: (a) Type 1; (b) Type 2; (c) Type 3; (d) Type 4.

Table 1. IPE-300 section properties.

IPE 300 Section Properties			AAC Mechanical Properties		
Total Depth	300	mm	Block Dimensions	600x250x120	mm
Top Flange Width	150	mm	Wall Thickness	125	mm
Top Flange Thickness	10.7	mm	Modulus of Elasticity	2250	N/mm²
Web Thickness	7.1	mm	Poission's Ratio	0.25	
Bottom Flange Width	150	mm	Compressive Strength	3.5	N/mm²
Bottom Flange Thickness	10.7	mm	Material Strength Class	G3	
Fillet Radius	15	mm	Unit Weight	600	kg/m³

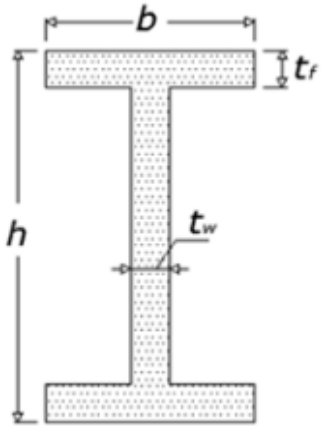

Fig. 6. IPE300 Section.

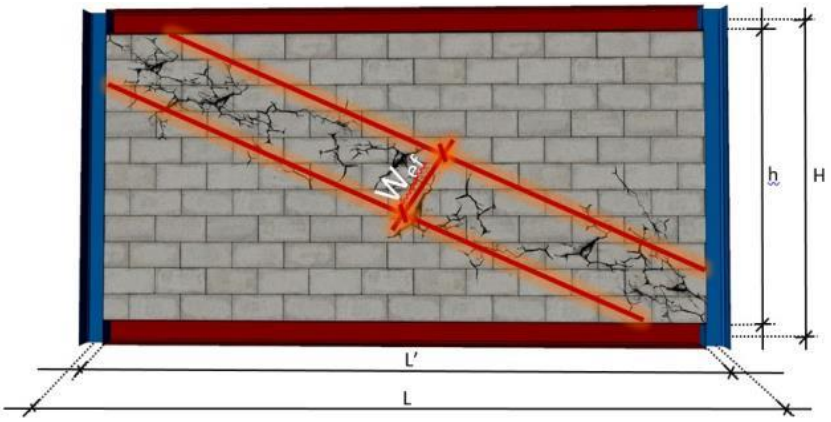

Fig. 7. Equivalent diagonal strut model.

Here, d: diagonal length, t: infill wall thickness, W_{ef}: effective wall thickness, E_m: infill wall elasticity module, E_s: frame elasticity module, H: story height, L: frame opening, L': wall opening, θ: horizontal angle of equivalent diagonal strut, I_c: column's moment of inertia. The numerical values of the diagonal properties of the infill wall were presented in Table 2.

In the examination, the horizontal earthquake force in x-direction has been taken into account whereas the effect of the walls in y-direction has been assessed only as weight. Four different frames have been modeled in ETABS software, non-linear analyses have been carried out under growing earthquake force, and the results have been compared. Evaluation of analysis results four different steel frames comprised of various combinations with infill walls have been modeled in ETABS software and pushover analyses have been performed. The displacements of the models examined which have occurred under the horizontal earthquake force are presented in Figs. 8a-d.

As seen in Figs. 8a-b, Type 2, consisting of infilled steel frames, has more stiffness and increases strength when compared to Type 1 whose frames without infill walls. Fig 8c shows Type 3, in which the basement floor is without infill walls because of various reasons such as commercial purposes and architectural decisions; the floor without infill walls behaves like a soft story under the earthquake force, and the infilled upstairs moves as a whole. In the frame of Type 4 torsion has been observed in which infill walls are distributed asymmetrically (Fig. 8d). The plastic hinges in the frames that have formed under controlled earthquake force have been presented in Fig. 9.

Table 2. Infill wall diagonal properties.

Type	h		λ		W_{ef}	
	Story 1	Story 2	Story 1	Story 2	Story 1	Story 2
	cm	cm	1/cm	1/cm	cm	cm
Type 1	285	270	0.011037298	0.010885136	46.24	46.00
Type 2	285	270	0.011037298	0.010885136	46.24	46.00
Type 3	285	270	0.011037298	0.010885136	46.24	46.00
Type 4	285	270	0.011037298	0.010885136	46.24	46.00

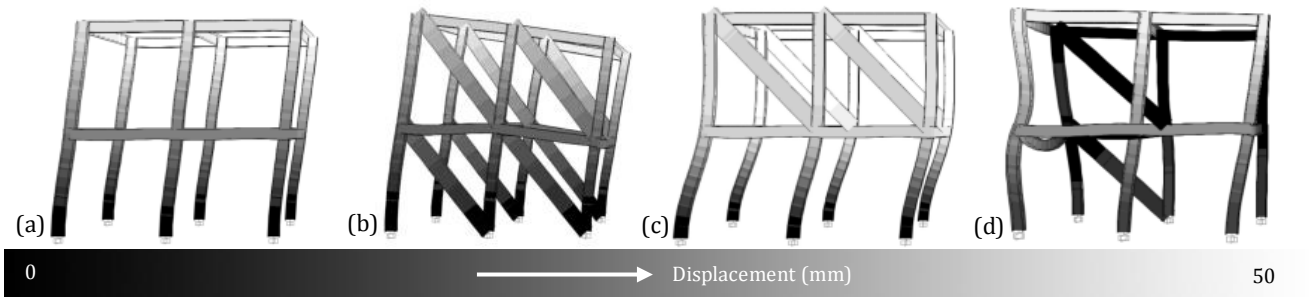

Fig. 8. Displacements due to horizontal load in: (a) Type 1; (b) Type 2; (c) Type 3; (d) Type 4.

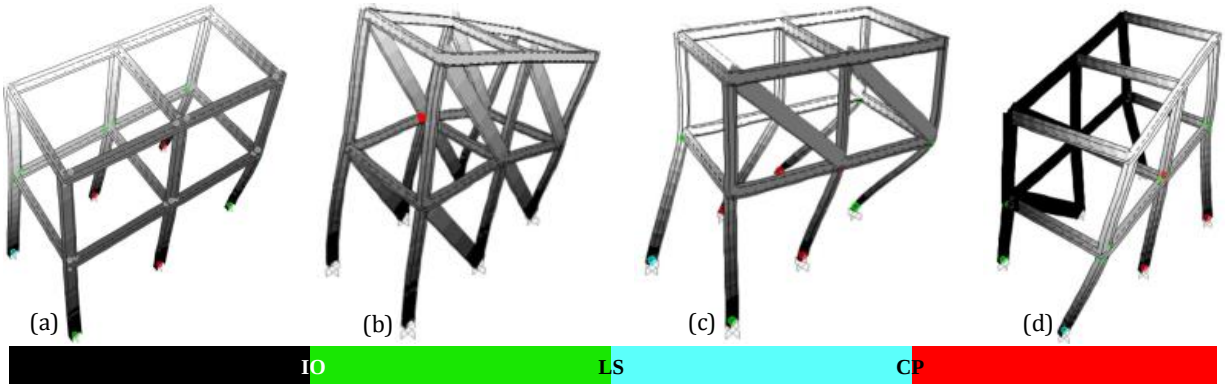

Fig. 9. Plastic hinges in the frames: (a) Frames without infill walls; (b) Frames with infill walls; (c) Effect of soft story; (d) Plastic hinges in asymmetrically distributed infill models.

While the plastic hinges have spread properly in two stories in Type 1, the plastic hinges have formed in the basement floor without walls in Type 3 which is under the effect of soft story (Figs. 9a, c). Since there are not many plastic hinges in Type 2; however, in Type 4, it has been observed that plastic hinges have concentrated in frames which having no infill and failure mechanism has formed (Figs. 9b, d). As a result of the analyses performed for all the cases under the horizontal load, the base shear force and top displacement correlation are shown in Fig. 10a and the maximum story displacements are presented in Fig. 10b.

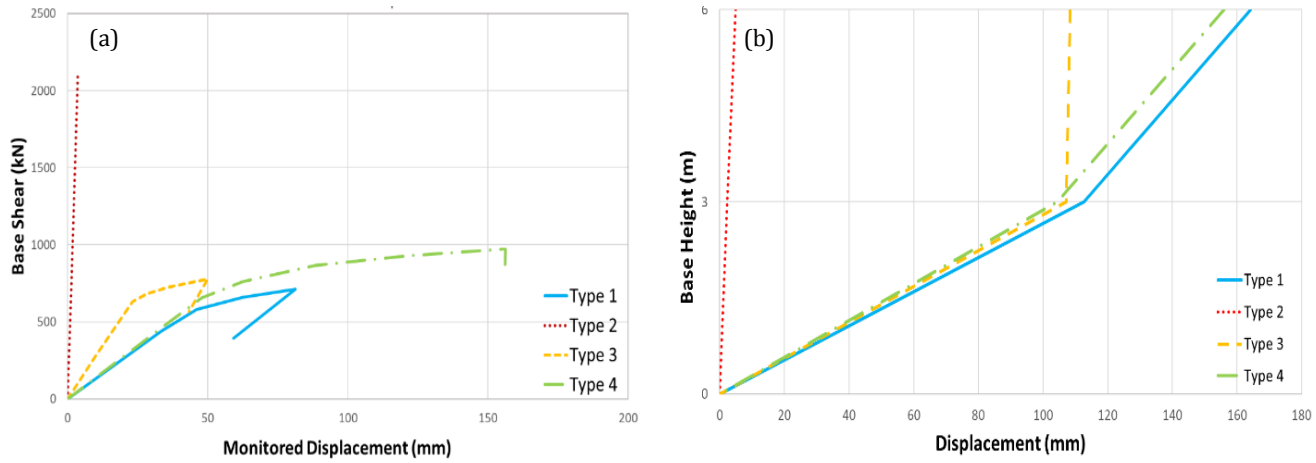

Fig. 10. (a) Base shear force and top displacement; (b) Maximum story displacement.

As is seen in Fig. 10, while the infill walls limit displacement in Type 2 which composed of symmetrical and fully infilled frames, plastic deformations are seen in other cases. In Type 3 with infill walls only in upper story, less displacement was observed in comparison with Type 1 consisting of bare frames due to stiffness of infill walls and weight. As for the Type 4, where there are asymmetrical infill walls in each story, the infill walls have caused torsion in the structure, which has led to even more displacement.

3. Conclusions

Infill walls support the steel frames by increasing the stiffness and strength under earthquake loads. Because of that contribution of infills walls is considered as to be on safe side and positive reserve, the effect of infill walls on structural system is ignored in design. However, infill walls might also lead to some irregularities in the structure, since placing infill walls asymmetrically in vertical and horizontal directions causes certain changes in the stiffness and strength of the structure. That's why, in the draft of 2016 Turkish Earthquake Code, using flexible joint connection between these two elements is stated as an option in order to minimize the effect of brittle infill walls on ductile frames.

In this study, to investigate the effect of infill walls on steel frame structures, four different cases have been determined and their pushover analyses have been performed. As a result of the analyses, it has been determined that infill walls increase strength and limit displacements. Yet, it has also been seen that placing infill walls asymmetrically in vertical and horizontal directions may lead to some irregularities such as soft story and torsion. Steel frames that are structurally far more ductile than infill walls cause deformations under horizontal load, whereas infill walls limit this situation. However, when infill walls and steel frames which have different deformation properties come together, cracks might occur in joints unless necessary precautions are taken.

REFERENCES

Akkuzu AV (2007). Betonarme Çerçeveli Dolgu Duvarların Deprem Etkisi Altındaki Dinamik Davranışının İncelenmesi. *M.Sc. Thesis*, İstanbul Technical University, İstanbul, Turkey.

Anıl Ö, Altın S (2007). An experimental study on reinforced concrete partially infilled frames. *Engineering Structures*, 29(3), 449-660.

Beklen C, Çagatay İH (2009). Çerçevelerde dolgu duvar modellerinin incelenmesi. *Çukurova University Journal of the Faculty of Engineering and Architecture*, 24(1-2), 1019-1011.

Beklen C (2009). Binalarda Dolgu Duvar Etkisinin İncelenmesi. *M.Sc. Thesis*, Çukurova University, Adana, Turkey.

DBYBHY (2007). Deprem bölgelerinde yapılacak binalar hakkında yönetmelik. Ministry of Public Works and Settlement, Ankara, Turkey.

Doğan O, Bakırcı Er Ş (2011). Hareketli yük ve dolgu duvar dağılımının burulma düzensizliğine etkisi. *International Journal of Engineering Research and Development*, 3(2), 2-5.

ETABS User's Manual. Integrated Building Design Software, Computer and Structure Inc. Berkeley, USA

FEMA-356 (2000). Prestandard and commentary for the seismic rehabilitation of buildings. Federal Emergency Management Agency, Washington, DC.

Ghaffarzadeh H, Ghalghachi RN (2009). Redundancy in steel frames with masonry infill walls. *World Academy of Science Engineering and Technology*, 3(10), 415-421.

İrtem E, Türker K, Hasgül U (2005). Dolgu duvarlarının betonarme bina davranışına etkisi. *İTÜ Journal: D-Engineering*, 4(4), 3-13.

Kaltakcı MY, Köken A, Korkmaz HH, Kamanlı M (2006). Dolgu duvarlı çelik çerçevelerin tersinir-tekrarlanır yükleme altındaki davranışı üzerinde deneysel bir çalışma. *Journal of the Engineering and Architecture Faculty of Selcuk University*, 21(1-2), 34-48.

Kaplan SA (2008). Dolgu duvarların betonarme taşıyıcı sistem performansına etkisi. *Türkiye Mühendislik Haberleri*, 6(452), 49-62.

Kaymak F, Tuna E (2012). Bant pencereli ve tam dolgu duvarlı çelik çerçevelerin yanal monotonik yükleme etkisi altında lineer elastik hesabı. *Journal of the Faculty of Engineering and Architecture of Gazi University*, 27(3), 547-556.

Mehrabi AB, Shing PB, Schuller MP, Noland JL (1996). Experimental evaluation of masonry-infilled RC frames. *Journal of Structural Engineering*, 122(3), 228-237.

Murty CVR, Jain SK (2000). Beneficial influence of masonry infill walls on seismic performance of RC frame buildings. *Proceedings of 12th World Conference on Earthquake Engineering*, Auckland, New Zealand, 1-6.

Öktem O (2003). Betonarme Çerçeve Sistemlerin Lineer Olmayan Hesabı ve Dolgu Duvarın Modellenmesi. *M.Sc. Thesis*, İstanbul Technical University, İstanbul, Turkey.

Sevil T, Baran M, Canbay E (2010). Tuğla dolgu duvarların B/A çerçeveli yapıların davranışına etkilerinin incelenmesi; deneysel ve kuramsal çalışmalar. *International Journal of Engineering Research and Development*, 2(2), 35-42.

Tabeshpour MR, Azad A, Golafshani AA (2012). Seismic behavior and retrofit of infilled frames in Earthquake-Resistant Structures - Design, Assessment and Rehabilitation, Moustafa A Ed., InTech, Croatia.

TBDY (2016). Türkiye Bina ve Deprem Yönetmeliği. Ministry of Environment and Urbanization, Ankara, Türkiye.

Yadollahi YY, Benli A, Varolguneş S (2016). Masonry infill walls effect in short column formation in RC buildings: Acase study. *Kahramanmaras Sutcu Imam University Journal of Engineering Sciences*, 19(2), 78-83.